The Impact of Terrain Sampling Density on 5G NR-V2X Downlink Channel Modeling Using Various Propagation Models at the 3.6 GHz Band

Tamas Istvan UNGER, Miklos KUCZMANN

Doctoral School of Multidisciplinary Engineering Sciences (MMTDI), Széchenyi István University, Egyetem tér 1., H-9026 Győr, Hungary

unger.tamas@nmhh.hu, kuczmann@ga.sze.hu

Submitted August 29, 2025 / Accepted October 9, 2025 / Online first November 5, 2025

Abstract. *This study investigates the sensitivity of radio wave propagation models to terrain sampling density in a 5G New Radio Vehicle-to-Everything downlink scenario at 3.6 GHz. Four widely used models are analysed: the empirical ITU-R P.1546-6, the deterministic Parabolic Equation Method, and the hybrid ITU-R P.1812-6 and ITU-R P.452-16. Real terrain profiles from Hungary are considered at multiple resolutions, allowing a systematic assessment of how accuracy degrades as the representation of terrain becomes coarser. The analysis reveals a consistent ranking across environments: the empirical model is the least affected by resolution changes, while deterministic and hybrid methods are significantly more sensitive. To interpret these differences, the study introduces a spectral complexity measure of terrain profiles and establishes its strong relationship with error growth through regression analysis. This provides a novel framework for explaining and quantifying the impact of terrain detail on model behaviour. The findings highlight both the methodological contribution of linking spectral complexity to propagation accuracy and the practical implications for optimising the trade-off between computational efficiency and prediction reliability in vehicular network planning.*

Keywords

Outdoor wave propagation models, terrain sensitivity, radio frequency electromagnetic waves, path loss prediction, channel modeling, vehicle-to-everything communications

1. Introduction

The modeling of electromagnetic wave propagation plays a pivotal role in the design and implementation of wireless communication systems. These models enable the estimation of propagation losses in the transmission medium without the need for on-site measurements, allowing for coverage planning and cost-effective network design prior to deployment [1]. Moreover, they are essential for assessing the compatibility of various telecommunication technologies, both within national borders and across them. In light of the rapid development of mobile communication systems and the increasing use of higher frequency bands, evaluating the accuracy of existing propagation models for new technologies and frequency ranges, as well as developing modern, advanced models, constitutes a timely and significant area of research [2].

To gain a first-order understanding of the general structure and operation of wave propagation models, it is useful to abstract the problem. Any propagation model may be regarded as a system with n direct inputs $(x_1, x_2, x_3, \ldots, x_n)$ and m so-called tuning parameters $(y_1, y_2, y_3, \ldots, y_m)$, whose characteristic outputs are the path loss and the absolute value of the resulting electric field strength. The system and two representative examples of its outputs are presented in Fig. 1.

Based on the above, the wave propagation model as a system can be formalized as

$$\Gamma\,(y_1, y_2, y_3, \ldots, y_m)\,\{x_1, x_2, x_3, \ldots, x_n\} \qquad (1)$$

where the outputs depend on both sets of input parameters. It is worth noting that the path loss determined at a given height above the ground and the electric field strength level are interconvertible, with the relationship between them governed by the expression:

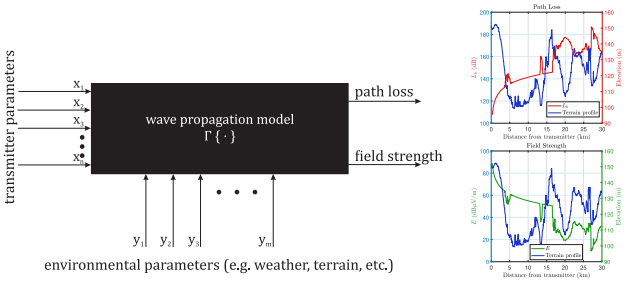

Fig. 1. The system model of a wave propagation model.

DOI: 10.13164/re.2025.0603

$$E = \mathrm{ERP} - L + 10\log_{10} f + 79.35 \qquad (2)$$

where E is the electric field strength in dBμV/m, ERP is the effective radiated power of the transmitter in dBm, L is the basic transmission loss in dB, and f is the frequency in MHz [3].

Propagation models are commonly classified into three major categories: purely empirical models based on observed data (typically measurement results); deterministic models founded on physical laws (e.g., the full set of Maxwell's equations); and hybrid models that combine elements of both approaches [4]. In this paper, we examine widely used and accessible models from each of these categories.

The 5G New Radio Vehicle-to-Everything (5G NR-V2X) systems [5] are communication technologies that enable real-time interaction between vehicles, road infrastructure, pedestrians, and the network [6]. The stability and reliability of these systems are of paramount importance and fundamentally depend on the quality of wireless links, especially in areas with varying terrain conditions. Therefore, the design of such networks requires the application of accurate and reliable radio wave propagation models, along with the understanding of their limitations [7]. In this paper, we focus exclusively on the analysis of downlink communication between the base station and the vehicle within the 5G NR-V2X system. The base station is considered as the transmitter, positioned at an average height of 30 meters above ground level, while the vehicle is treated as the receiver, with an antenna height of 1.5 meters above the ground. This case is illustrated in Fig. 2.

One of the most critical tuning parameters in propagation models is the terrain profile between the transmitting antenna and the receiver [8]. It is evident that the terrain characteristics along the analyzed propagation path significantly influence the propagation phenomena, such as diffraction, multipath propagation, or determining whether line-of-sight conditions are met. Therefore, accurately defining the terrain is essential for achieving precise simulation results. On the other hand, a more accurate (i.e., more densely sampled) terrain profile increases computational demands, thus reducing the efficiency of propagation model algorithms. This raises the need to achieve the desired level of computational accuracy with the sparsest possible terrain sampling. Our research aims to investigate, through a 3.6 GHz 5G NR-V2X downlink link, how the degradation in terrain sampling density affects the computational accuracy of several commonly used propagation models applicable to this frequency band. Recognizing that the choice of interpolation between known discrete terrain points may affect accuracy [9], linear interpolation is adopted throughout this study in order to ensure methodological simplicity and consistency; the impact of alternative interpolation methods on accuracy is not considered.

As an example, Fig. 3 presents a specific terrain profile under linear interpolation, illustrating the effects of varying sampling densities.

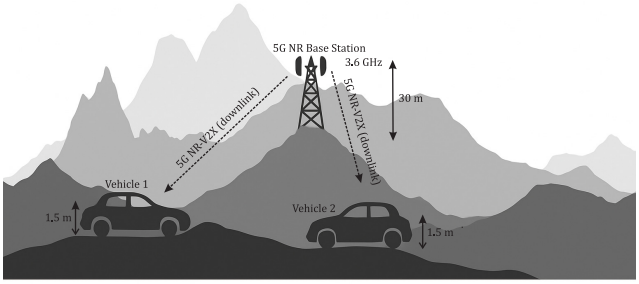

Fig. 2. The downlink connection of the 5G NR-V2X system.

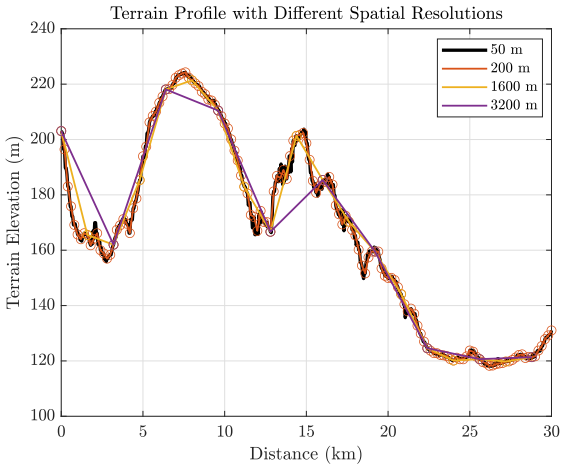

Fig. 3. Effect of spatial resolution on terrain profile representation.

In the scope of this article, we examine four different radio wave propagation models: the ITU-R P.1546-6 model, which is a widely adopted empirical method; the Parabolic Equation Modeling (PEM) approach as a deterministic example; and the ITU-R P.452-16 and P.1812-6 models, both of which represent hybrid approaches. The analysis is carried out in the 3.4–3.8 GHz frequency band, which has been harmonized within the European Union for terrestrial systems capable of providing electronic communications services [10], with specific frequency arrangements and technical conditions defined in ECC Decision (11)06 [11]. This band is allocated on a co-primary basis to mobile services (excluding aeronautical mobile) according to the Radio Regulations (RR) [12], and is designated for mobile use in the European Table of Frequency Allocations and Applications (ECA Table) [13]. Its favorable balance between coverage and capacity, along with regulatory harmonization, makes it a suitable candidate for 5G NR-V2X deployments, and therefore a relevant choice for propagation modeling in this study.

Building on our previous study, which provided a comparative evaluation of empirical, hybrid, and deterministic propagation models in the 3.6 GHz and 6 GHz frequency bands [3], the present work advances this line of research

in several important ways. While the earlier analysis focused primarily on the overall prediction accuracy and general applicability of the models under different frequency conditions, it did not address their sensitivity to terrain representation and its sampling density.

In contrast, this study systematically investigates how variations in the spatial resolution of digital elevation data influence path loss estimation and the stability of model outputs. By quantifying the terrain-sampling dependence of each model, we reveal significant differences in how empirical, hybrid, and deterministic approaches respond to changes in input granularity.

This sensitivity-oriented perspective not only deepens the understanding of model behavior under realistic geographic conditions but also provides practical guidance for selecting appropriate terrain resolutions in large-scale propagation simulations.

The remainder of this paper is structured as follows. Section 2 provides an overview of the state of the art in outdoor propagation modeling, highlighting the lack of studies addressing the sensitivity of model accuracy to terrain sampling density. Section 3 details the adopted methodology, as well as the design of controlled test cases over three representative Hungarian regions. Section 4 presents the simulation results and evaluates how terrain sampling density affects the accuracy of each model. Section 5 introduces the spectral complexity ratio as a new terrain-dependent indicator and demonstrates its strong exponential correlation with the average RMSE. Finally, Section 6 summarizes the findings and discusses their implications for future 5G/6G network planning and spectrum management.

2. State of the Art and Research Gap

Accurate and reliable channel modeling is essential for the design and optimization of 5G NR-V2X systems, especially at 3.6 GHz, which serves as a primary frequency band for vehicular and intelligent transportation networks. The spatial resolution of terrain data (referred to as terrain sampling density) plays a decisive role in determining how effectively a propagation model can represent diffraction, shadowing, and multipath propagation effects [14]. Higher terrain sampling density allows the model to capture small-scale topographic variations that influence the received signal power and time–frequency dispersion of multipath components, particularly in complex or mountainous areas [15–17].

Earlier research provides a wide comparative background on model behavior under various topographical conditions. The ITU-R P.1546-6 model, while widely adopted for large-scale coverage estimation, tends to overestimate near base stations and underestimate signal levels in rural or obstructed environments [17–19]. The Parabolic Equation Method, introduced by Levy [20] and refined by Donohue and Kuttler [21], numerically solves the wave equation for irregular terrain, offering high fidelity in diffraction and shadow region modeling but at the expense of computational intensity. Hybrid models such as ITU-R P.452-16 and ITU-R P.1812-6 bridge empirical and deterministic approaches, maintaining good accuracy in moderately complex terrain while remaining computationally efficient [3]. However, these models still experience performance degradation in highly rugged environments due to simplified diffraction approximations.

Several works have addressed terrain-induced diffraction and multipath effects through enhanced numerical schemes and ray-tracing validations [22–26]. For instance, PE-based simulations can handle slope angles up to 20°, providing consistent results with both theoretical and empirical observations. Meanwhile, hybrid models like ITU-R P.452-16 employ multi-knife-edge diffraction methods [27], which balance computational load with acceptable accuracy for large-scale network planning. Despite these advances, most studies still focus on urban, highway, or relatively flat rural regions, with mountainous and highly rugged terrains largely underrepresented in the literature [16, 28, 29].

Beyond topographical sensitivity, methodological progress has been achieved through the use of geometry-based deterministic and hybrid frameworks. Studies leveraging models such as Geometry-based Efficient propagation Model for ehicle-to-Vehicle and ehicle-to-Infrastructure communications (GEMV^2) and Three-Dimensional Geometry-based Stochastic Vehicle-to-Vehicle Channel Model (3D-GSV^2) integrate digital terrain and obstacle information to classify link types and simulate fading mechanisms [30], [31]. These approaches demonstrate that detailed environmental geometry – including vehicle outlines, foliage, and building density – strongly influences delay spread, shadow fading, and overall channel reliability.

Although numerous studies have compared propagation models under specific scenarios, few have systematically examined how the *terrain sampling density* – that is, the spatial resolution of digital elevation data – affects the predictive performance and computational efficiency of different propagation models. Most existing works focus on individual model validation or frequency-specific case studies, but they do not analyze the interplay between terrain discretization and model behavior under identical simulation conditions, particularly at mid-microwave frequencies such as 3.6 GHz and 6 GHz.

Furthermore, the literature lacks a quantitative assessment of how empirical models (e.g., ITU-R P.1546-6) and hybrid or deterministic approaches (e.g., ITU-R P.452-17 and PEM) respond to varying terrain resolutions when all other environmental and simulation parameters are held constant.

Consequently, the sensitivity of propagation loss predictions to terrain sampling density remains poorly understood, despite its critical importance in the design of accurate, scalable, and reproducible radio-propagation simulations.

The present study aims to fill this gap by conducting a comprehensive and controlled comparison of three major outdoor propagation models – ITU-R P.1546-6, ITU-R P.452-17, and the Parabolic Equation Method (PEM) – across multiple terrain configurations and sampling densities. By quantifying the variations in key performance indicators such as Root Mean Square Error (RMSE), Mean Absolute Error (MAE), and Bias between model outputs, the study provides insight into how digital elevation model (DEM) resolution impacts model accuracy and computational cost.

In addition, an automated simulation framework has been developed to ensure consistent pre-processing, terrain sampling, and model evaluation, thereby providing a reproducible benchmark for future research. This contribution helps clarify the terrain sensitivity of empirical, hybrid, and deterministic approaches, supporting both regulatory applications and next-generation 5G/6G system planning.

To further quantify the relationship between terrain characteristics and model accuracy, this study introduces the spectral complexity ratio (SCR) as a novel terrain descriptor. This, derived from the Fourier transform of the elevation profile, expresses the proportion of high-frequency terrain components relative to the total spectral energy, thus providing a compact indicator of topographic irregularity. Unlike terrain sampling density, which only defines the spatial resolution of input data, the SCR directly characterizes the morphological complexity of the terrain itself.

By comparing the average root mean square error of propagation model predictions with the corresponding SCR values, a strong exponential correlation was identified across all models and frequency bands. This finding establishes a direct link between the spectral complexity of the terrain and the expected model error, enabling the a priori estimation of the model uncertainty without extensive simulations. The proposed approach therefore provides a physically interpretable and computationally efficient framework for assessing model reliability as a function of terrain complexity.

3. Methodology

In the present study, we examine the above mentioned four radio wave propagation models based on different theoretical foundations. The accuracy of the models in the function of terrain sampling density is assessed using real topographic data from Hungary, considering three distinct scenarios: an urban hilly area, a flat terrain, and a mountainous region. For each case, both low-density test point evaluations and high-resolution line-based calculations are carried out.

The aim of the analysis is to evaluate how the accuracy of these models depends on the terrain sampling density, specifically in the context of a 3.6 GHz 5G NR-V2X downlink application.

3.1 Wave Propagation Models

To demonstrate the differences between the investigated models, Figure 4 presents the results of line-based calculations along the same terrain profile using the ITU-R P.1546-6, PEM, ITU-R P.452-16, and ITU-R P.1812-6 methods. A side-by-side comparison reveals substantial variations between the models, as well as the differing degrees to which terrain characteristics influence the outcomes. While a comprehensive accuracy assessment of these approaches is beyond the scope of this paper, further details on their comparative performance can be found in the relevant literature [3].

Among the examined models, ITU-R P.1546-6 [32] is an empirical point-to-area propagation model developed for frequencies between 30 MHz and 4000 MHz, suitable for various terrestrial services. It relies on interpolation and extrapolation from field strength curves derived from extensive measurement data, incorporating parameters such as distance, frequency, antenna height, time, and location variability.

The model includes corrections for terrain clearance, clutter, mixed land-sea paths, and antenna height differences, making it adaptable to diverse environments, particularly for long-range scenarios up to 1000 km. Due to its wide acceptance and standardized methodology, it provides a robust reference for evaluating terrain-dependent propagation behavior.

The Parabolic Equation Modeling approach employed in this study is a deterministic numerical method that solves a form of the parabolic approximation to the Helmholtz equation, enabling accurate modeling of wave diffraction, refraction, and terrain-induced scattering in complex environments. Using the Split-Step Fourier Method [33] or the Crank-Nicolson Method [34], PEM computes the field propagation in a terrain-following two-dimensional grid.

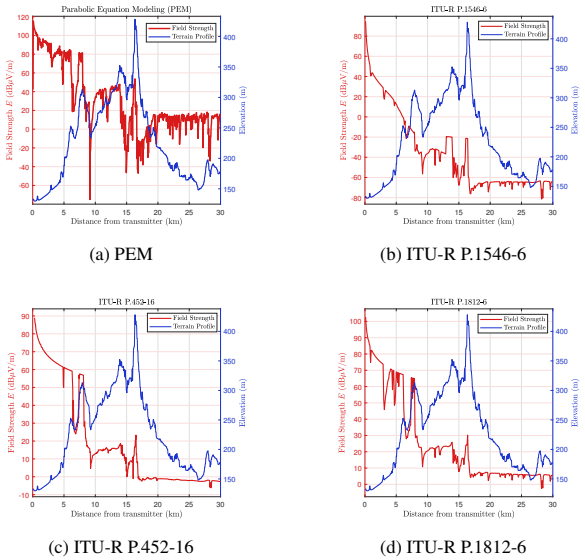

(a) PEM (b) ITU-R P.1546-6

(c) ITU-R P.452-16 (d) ITU-R P.1812-6

Fig. 4. Line-based examples for the investigated models.

The key relation,

$$\frac{\partial \psi(x,z)}{\partial x} = -\frac{\mathrm{j}}{2k_0}\left(\frac{\partial^2 \psi(x,z)}{\partial z^2} + k_0^2\left(n^2-1\right)\psi(x,z)\right), \quad (3)$$

describes the evolution of the complex field $\psi(x,z)$ in the range-height domain, where k_0 is the free-space wave number and n is the refractive index profile [35]. This formulation allows terrain effect to be incorporated via boundary conditions and terrain-following coordinate transformations.

The ITU-R P.452-16 is a semi-deterministic point-to-point propagation model designed to predict interference and wanted signal levels from 100 MHz. It incorporates multiple propagation mechanisms including line-of-sight, diffraction over terrain obstacles, tropospheric scatter, and anomalous propagation such as ducting and layer reflection based on detailed terrain and atmospheric refractivity profiles. The model uses digital elevation data and climatic parameters to estimate path-specific losses under varying time percentages. It supports the assessment of both short- and long-range paths and is particularly suited for frequency coordination, interference analysis, and high-frequency backhaul planning [36].

Last, but not least the ITU-R P.1812-6 is a point-to-area and point-to-point propagation model specifically developed for frequencies from 30 MHz to 6 GHz, optimized for terrestrial services in mixed urban, suburban, and rural environments. It combines empirical and deterministic elements, incorporating terrain data, land cover classification, and statistical parameters to estimate path loss with high spatial resolution. The model supports various propagation mechanisms, including line-of-sight, diffraction over terrain and buildings, and tropospheric effects, and is designed to handle irregular topographies and clutter conditions [37]. By integrating both digital elevation models and clutter height databases, it offers detailed predictions for coverage, interference, and compatibility analyses. Within the present study, ITU-R P.1812-6 contributes a hybrid approach that bridges the gap between purely empirical models and full-wave deterministic methods.

3.2 Test Cases

To comprehensively evaluate the degradation in accuracy of the investigated radio wave propagation models as a function of terrain resolution, two distinct test scenarios were devised. In the first scenario, we employed version 7.5.1.1 of the LStelcom CHIRplus_BC broadcast network planning tool software [38], which incorporates all the propagation models under study–except for the Parabolic Equation Method (PEM)–and features its own terrain database with a maximum resolution of 50 meters.

As illustrated in Fig. 5, the selected test areas are shown within the simulation software environment.

Three separate 900 km^2 regions were defined across Hungary to represent distinct geographic environments: one in and around Budapest, characterizing an urban, hilly setting; another in the Great Hungarian Plain near Kecskemét, representing flat terrain; and a third in close proximity to Kékestető, Hungary's highest peak, illustrating a mountainous and highly fragmented region. In each of these areas, a 5G New Radio (5G NR) base station with a reference height of 30 meters was placed in the bottom-right corner; for the Kékestető area, the station was positioned directly on the mountaintop. Subsequently, 30 test points were distributed across each region. These points were assigned a height of 1.5 meters above ground level, simulating the typical elevation of a vehicle-mounted receiver. At each test location, signal strength levels were evaluated. The terrain profiles are illustrated in Fig. 6 and the bounding World Geodetic System 1984 (WGS84) coordinates of the areas are provided in Tab. 1.

Area type	$X_{\min}$	$Y_{\min}$	$X_{\max}$	$Y_{\max}$
Urban, hilly	18.3602	47.3146	19.0400	47.7366
Flat	19.7074	46.4795	20.3982	46.8978
Mountainous	19.6992	47.7689	20.2966	48.1322

Tab. 1. The WGS84 coordinates of the limits of the areas (CHIRplus_BC).

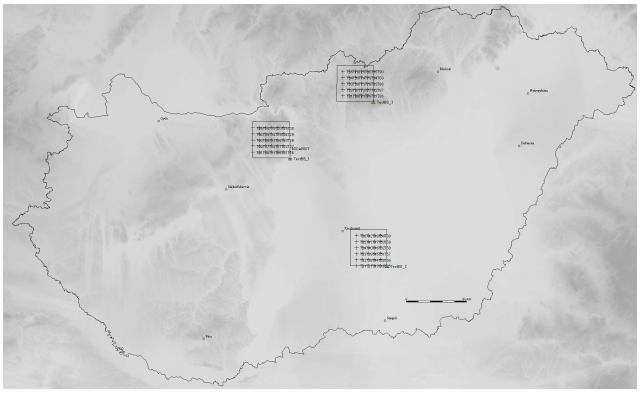

Fig. 5. The point-based test cases in CHIRplus_BC software.

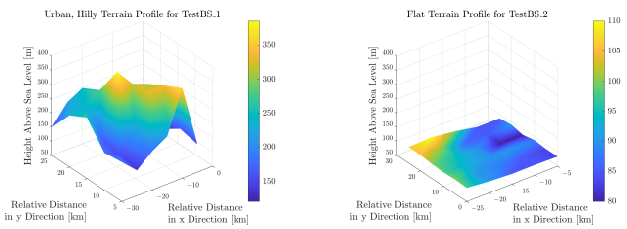

(a) Urban, hilly (b) Flat

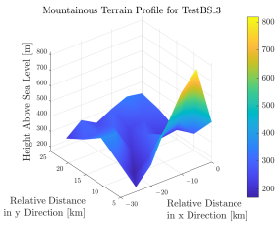

(c) Mountainous

Fig. 6. Terrain profiles of the defined areas in CHIRplus_BC.

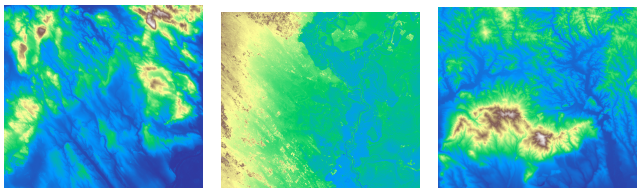

(a) Urban, hilly (b) Flat (c) Mountainous

Fig. 7. Color relief map of the areas (OpenTopography).

Area type	X_{min}	Y_{min}	X_{max}	Y_{max}
Urban, hilly	18.6855	47.4355	19.0893	47.7036
Flat	19.7771	46.6554	20.1738	46.9209
Mountainous	19.5988	47.8726	20.0078	48.1379

Tab. 2. The WGS84 coordinates of the limits of the areas (OpenTopography).

Metric	Urban, hilly	Flat	Mountainous
Min [m]	93	66	100
Max [m]	761	141	1034
Elevation range [m]	669	75	934
Mean [m]	228	90	308
Standard deviation [m]	97	10	139
Mean slope	2.9	0.7	4.7

Tab. 3. Key statistical parameters of the three terrain profiles.

In the second scenario, we relied on the freely available Copernicus GLO-30 Digital Elevation Model, obtained through the OpenTopography platform [39]. In this case, three areas are again examined, selected to match the characteristics of the regions used in the test point-based calculations. The bounding coordinates of these areas are provided in Tab. 2, their terrain characteristics are summarized in Tab. 3, and the areas are illustrated in Fig. 7.

From these areas, 200 terrain profiles of 30 km in length were randomly extracted using a custom Python script. To enable the batch processing of these profiles, a dedicated iterative script was developed in MATLAB [40] to interface with the implemented versions of the ITU-R P.1546-6, ITU-R P.1812-6, and ITU-R P.452-16 propagation models available online [41]. These terrain profiles were then processed under varying resolution settings, yielding line-based simulation results with a significantly larger sample size than those produced by the test point-based method.

The PEM approach constitutes an exception in both the test point-based and line-based simulations, as the PEM simulations were carried out using the PETOOL v2.0 MATLAB toolbox [42]. This toolbox cannot be directly integrated with CHIRplus_BC and is primarily operated through its own graphical user interface. As a first step, we reverse-engineered the PETOOL code and developed an iterative script that directly calls the Split-Step Parabolic Equation (SSPE) function marked as `SSPE_function()`, responsible for the core computations. This custom script enabled the efficient batch processing of line-based calculations. For the test point-based simulations, the terrain profiles between the test base station and the respective test points were exported from CHIRplus_BC and processed similarly using the line-based method. However, only the result corresponding to the final point along each path (that is, the test point itself) was retained for analysis.

For the sake of straightforward comparability and to eliminate confounding factors in the assessment of model accuracy, the 5G NR test base stations under investigation were equipped with omnidirectional antennas. Their average effective radiated power was 46 dBm, and the transmission frequency was set to 3.6 GHz [43].

3.3 Terrain Downsampling and Calculation

To assess the sensitivity of radio propagation models to terrain data resolution, we applied a downsampling and interpolation-based methodology. This approach aims to quantify the extent to which the spatial resolution of input terrain data affects the accuracy of field strength predictions.

Let $h_{\text{ref}}[i]$ denote the reference terrain profile, composed of N regularly spaced elevation samples (e.g., at 30-meter intervals), which serves as the baseline for accurate modeling. The corresponding electric field strength profile $E_{\text{ref}}[i]$ is obtained by applying a selected propagation model using the full-resolution profile as input.

To simulate lower-resolution terrain input, we apply systematic downsampling to the reference profile by retaining every k-th sample:

$$h_{\text{thin}}[j] = h_{\text{ref}}[jk], \quad j = 0, 1, \ldots, \left\lfloor \frac{N}{k} \right\rfloor \tag{4}$$

where $k \in \mathbb{N}$ denotes the downsampling fator (e.g., $k = 2, 5, 10$). The resulting coarse profile is then linearly interpolated back to the original resolution in order to reconstruct a full-length approximation of the terrain:

$$h_{\text{interp}}[i] = h_{\text{thin}}[j] + \left(\frac{i - jk}{k}\right) \cdot \left(h_{\text{thin}}[j+1] - h_{\text{thin}}[j]\right), \quad \text{for } jk \le i < (j+1)\,k. \tag{5}$$

This interpolated profile $h_{\text{interp}}[i]$ is then used as the input for a new run of the propagation model to obtain a modified field strength profile:

$$E_{\text{interp}}[i] = \Gamma\left\{h_{\text{interp}}[i]\right\}. \tag{6}$$

The deviation introduced by terrain downsampling is then quantified by comparing the interpolated field strength profile to the reference profile using standard error metrics.

3.4 Metrics for Sensitivity Analysis

To evaluate the degradation in accuracy of the propagation models as a function of terrain resolution, several statistical metrics were employed [44]. Let E_i denote the reference

field strength value at the i-th point, obtained using the highest available terrain resolution, and let $\hat{E}_i$ be the corresponding predicted value obtained using a reduced-resolution terrain dataset. The total number of evaluation points or profiles is denoted by N. It is clear that the reference field strength vector and the field strength vectors corresponding to sparser terrain sampling have the same length, as the missing points are filled in using linear interpolation.

The Mean Absolute Error (MAE) quantifies the average magnitude of the absolute errors between predicted and reference values, irrespective of direction:

$$\mathrm{MAE} = \frac{1}{N}\sum_{i=1}^{N}\left|\hat{E}_i - E_i\right|. \tag{7}$$

The Root Mean Square Error (RMSE) places greater emphasis on larger errors due to the squaring and is sensitive to outliers:

$$\mathrm{RMSE} = \sqrt{\frac{1}{N}\sum_{i=1}^{N}\left(\hat{E}_i - E_i\right)^2}. \tag{8}$$

The Bias indicates whether the reduced-resolution terrain model systematically overestimates or underestimates the field strength:

$$\mathrm{Bias} = \frac{1}{N}\sum_{i=1}^{N}\left(\hat{E}_i - E_i\right). \tag{9}$$

It is also informative to examine the Standard Deviation of the Error (σ_e), which characterizes the variability of the errors around the mean value:

$$\sigma_\mathrm{e} = \sqrt{\frac{1}{N}\sum_{i=1}^{N}\left(\left(\hat{E}_i - E_i\right) - \mathrm{Bias}\right)^2}. \tag{10}$$

The pointwise relative error, denoted as RelErr_i, was calculated in the linear scale (i.e., in µV/m) rather than in the logarithmic dB scale. This approach ensures physical consistency, as the relative error inherently refers to a ratio between absolute field strength values. The relative error was computed only where the reference field strength was non-zero, according to the following formula:

$$\mathrm{RelErr}_i = \frac{\left|\hat{E}_i - E_i\right|}{|E_i|}\cdot 100\ \% \tag{11}$$

where E_i is the reference field strength and $\hat{E}_i$ is the predicted value, both expressed in µV/m. This method avoids division by zero and ensures meaningful percentage deviations are reported. Finally, the mean of all valid RelErr_i values was calculated for each resolution level.

Last, but not least, it is useful to define the normalized RMSE (nRMSE) which facilitates comparisons across datasets with differing dynamic ranges:

$$\mathrm{nRMSE} = \frac{\mathrm{RMSE}}{E_\mathrm{max} - E_\mathrm{min}} \tag{12}$$

where $E_\mathrm{max} - E_\mathrm{min}$ denote the maximum and minimum of the reference values, respectively.

3.5 Spectral-Driven Profile Simplification

To investigate how terrain sampling density affects propagation model outputs, we introduced a controlled procedure involving artificial downsampling of terrain profiles, followed by linear interpolation to restore the original profile length [45]. Field strength was then recalculated using the same propagation model, and compared to the reference results computed on the full-resolution terrain. This approach allowed us to isolate the effects of terrain resolution from other factors and quantify their impact on model accuracy.

To anticipate whether a given terrain profile is susceptible to accuracy loss under reduced sampling, we analysed its spatial frequency content using the discrete Fourier transform (DFT) [46]. Let the terrain be represented as discrete elevation sequence $z_n = z\,(n\cdot\Delta x)$, where Δx is the original sampling interval. The DFT of the "signal" is:

$$Z_\ell = \sum_{n=0}^{N-1} z_n \cdot \mathrm{e}^{-\mathrm{j}\frac{2\pi\ell n}{N}},\ \ell = 0,\ldots,N-1 \tag{13}$$

and the corresponding spectral power is:

$$S_\ell = |Z_\ell|^2. \tag{14}$$

The spatial frequency for each index is

$$f_\ell = \frac{\ell}{N\cdot\Delta x}. \tag{15}$$

To assess sensitivity to downsampling by a factor k, a cutoff frequency is introduced based on the Nyquist criterion for the reduced sampling interval $k\cdot\Delta x$:

$$f_\mathrm{c} = \frac{1}{2k\cdot\Delta x}. \tag{16}$$

Frequencies below f_c are retained after downsampling, while those above are lost or aliased. Accordingly, we compute the total energy in the low-frequency (LFE) and high-frequency (HFE) domains as:

$$\mathrm{LFE} = \sum_{f_\ell < f_\mathrm{c}} S_\ell,\ \mathrm{HFE} = \sum_{f_\ell \geq f_\mathrm{c}} S_\ell. \tag{17}$$

The spectral complexity ratio is then defined as:

$$R^{(k)} = \frac{\mathrm{HFE}}{\mathrm{LFE}+\mathrm{HFE}}. \tag{18}$$

This dimensionless parameter $R^{(k)} \in [0,1]$ quantifies the proportion of high-frequency energy in the terrain profile at a given downsampling factor k. Higher $R^{(k)}$ values indicate greater local variation and steeper slopes, suggesting higher sensitivity to profile simplification. To evaluate the predictive utility of $R^{(k)}$, the root mean square error (RMSE) has been calculated between the field strength calculated on the full-resolution profile and that obtained from the interpolated profile after downsampling. Each terrain segment was associated with a pair $\left(R_i^{(k)}, \mathrm{RMSE}_i^{(k)}\right)$.

Instead of analysing these pairs individually for all N_p profiles, we adopted an *aggregated analysis*: for each downsampling factor k, we averaged $R^{(k)}$ and $\mathrm{RMSE}^{(k)}$ across all $N_p = 200$ profiles, resulting in a single aggregated data point $\left(\overline{R}^{(k)}, \overline{\mathrm{RMSE}}^{(k)}\right)$. This reduces the influence of profile-specific variability and reveals the global trend between spectral complexity and model error as a function of terrain resolution.

The aggregated data points were first fitted with a simple linear regression model:

$$\overline{\mathrm{RMSE}}^{(k)} = \beta_0 + \beta_1 \overline{R}^{(k)} + \varepsilon^{(k)} \tag{19}$$

where β_0 is the intercept, β_1 is the slope, and $\varepsilon^{(k)}$ is the residual error term for downsampling factor k.

We also tested a saturating exponential model. To improve numerical stability, we min–max normalized the predictor

$$r^{(k)} = \frac{\overline{R}^{(k)} - R_{\min}}{R_{\max} - R_{\min}} \in [0, 1] \tag{20}$$

and fitted the following first-order (asymptotic) response model to the six aggregated points:

$$\overline{\mathrm{RMSE}}^{(k)} = c + A\left(1 - \mathrm{e}^{-B\, r^{(k)}}\right) + \varepsilon^{(k)}. \tag{21}$$

Parameters (c, A, B) were estimated by non-linear least squares (sum of squared errors) using derivative-free optimization with multiple reasonable initial values.

4. Test Point-Based Results

Our investigations based on test point simulations were carried out in the CHIRplus_BC environment, following the previously described methodology. For the ITU-R P.1546-6, ITU-R P.452-16, and ITU-R P.1812-6 propagation models, the time percentage was uniformly set to 10%, and the location percentage to 50%. In the case of the ITU-R P.452-16 model, the prediction type was set to "Average Year", while the surface parameters were configured as follows: temperature was set to 20°C, atmospheric pressure to 1013.25 hPa, and water vapour density to 8 g/m^2; the atmospheric refractivity (N_0) was set to 330 N-units, and the refractivity index lapse rate to 45 N-units/km. The same parameters were applied in the ITU-R P.1812-6 model and during the line-based computations to ensure comparability.

4.1 Urban, Hilly Terrain

The metrics calculated from the simulation results for urban, hilly terrain are presented in Tab. 4 and Fig. 8. The results corresponding to the 50 m raster resolution serve as the reference, against which the calculations performed using coarser terrain profiles were compared. The performance of the ITU-R P.452-16 model across varying terrain resolutions in urban, hilly environment reveals a generally consistent and interpretable pattern. At the finest resolutions (100 m and 200 m), the model demonstrates high accuracy, with MAE values of 0.70 and 0.62 dBµV/m, respectively, and RMSE values of 1.26 and 1.13 dBµV/m. The relative error remains modest at 6.10% and 4.36%, while the normalised RMSE (nRMSE) is below 0.02 in both cases, confirming strong alignment with the reference results.

From 400 m upwards, however, a clear decline in accuracy is observed. The RMSE at 400 m rises sharply to 6.83 dBµV/m, accompanied by a relative error of 19.87%. Despite a temporary decrease in RMSE at 800 m (to 5.30 dBµV/m), the relative error escalates to 39.96%, indicating non-linear error amplification due to increased terrain generalization.

At 1600 m resolution, all error metrics deteriorate significantly, with the RMSE reaching 12.10 dBµV/m and the relative error exceeding 369.64%. These results confirm that the P.452-16 model is highly sensitive to terrain resolution, particularly beyond 200 m, and may produce unreliable estimates when applied to coarse digital elevation models in complex urban or hilly environments.

The ITU-R P.1546-6 model demonstrates a relatively stable performance across different terrain resolutions, although with clear signs of sensitivity at coarser levels. At the finest resolution (100 m), its MAE and RMSE values are 1.52 and 2.98 dBµV/m, respectively, with a linear relative error of only 1.16%. These values indicate that, despite being higher than those of P.452-16, the model maintains good absolute and relative accuracy in densely sampled terrains.

Test-point results: Urban, hilly terrain						
Resolution	**MAE** [dB]	**RMSE** [dB]	**Bias** [dB]	σ_e [dB]	**RelErr** [%]	**nRMSE** [–]
ITU-R P.452-16						
100 m	0.697	1.263	–0.037	1.262	6.10	0.0187
200 m	0.620	1.134	0.347	1.079	4.36	0.0168
400 m	2.377	6.827	–0.403	6.815	19.87	0.1013
800 m	2.843	5.295	0.743	5.243	39.96	0.0786
1600 m	6.363	12.100	1.310	12.029	369.64	0.1795
ITU-R P.1546-6						
100 m	1.520	2.975	0.207	2.968	1.16	0.0366
200 m	1.527	2.820	0.707	2.730	2.34	0.0347
400 m	3.037	5.319	0.650	5.279	20.30	0.0655
800 m	3.293	5.421	2.420	4.850	6.17	0.0668
1600 m	6.830	8.995	4.183	7.963	39.21	0.1108
ITU-R P.1812-6						
100 m	0.690	1.260	–0.043	1.259	8.42	0.0188
200 m	0.597	1.110	0.343	1.055	7.72	0.0165
400 m	2.377	6.811	–0.383	6.800	20.14	0.1015
800 m	2.823	5.278	0.743	5.226	34.02	0.0787
1600 m	6.337	12.053	1.390	11.973	223.97	0.1796
PEM						
100 m	6.911	11.340	1.890	11.181	94.66	0.0737
200 m	8.548	10.464	2.992	10.027	164.41	0.0680
400 m	15.823	20.805	8.828	18.839	817.42	0.1352
800 m	15.674	21.692	9.612	19.446	1003.9	0.1410
1600 m	26.973	36.396	16.987	32.189	2287.3	0.2365

Tab. 4. Test point-based error metrics in urban, hilly environments.

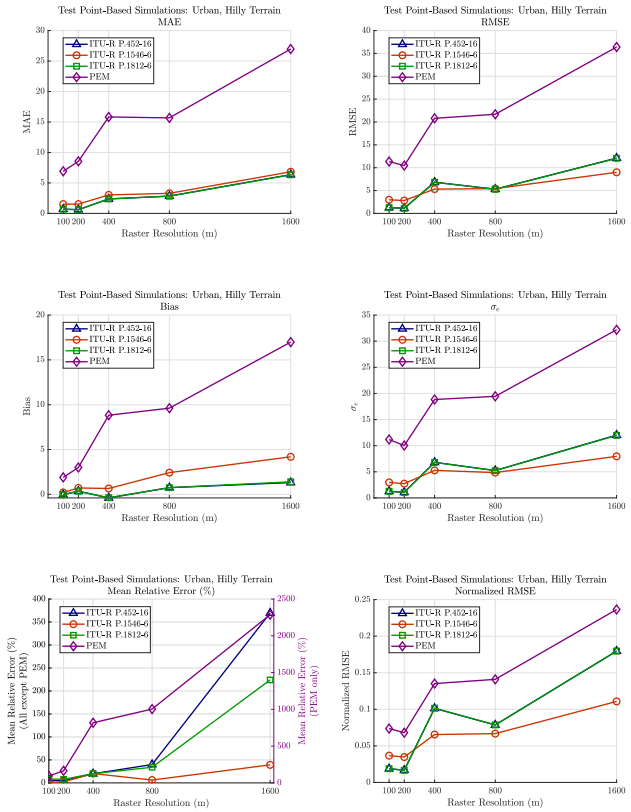

Fig. 8. Test point-based error metrics of simulations over urban, hilly terrain at varying terrain resolutions.

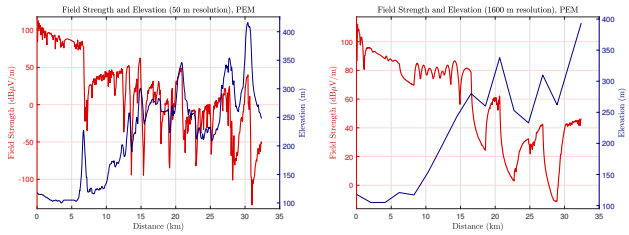

Fig. 9. PEM calculations from the base station to a testpoint.

At 200 m resolution, the results remain remarkably consistent: MAE and RMSE change only marginally (1.53 and 2.82 dBμV/m), and the relative error increases slightly to 2.34%. This suggests that moderate terrain simplification does not substantially affect the model's prediction accuracy. However, from 400 m onwards, a more pronounced degradation emerges. At 400 m, RMSE increases to 5.32 dBμV/m and relative error surges to over 20%, reflecting a drop in robustness. This is followed by a non-monotonic trend: at 800 m resolution, although the bias increases sharply to 2.42 dB, the standard deviation (σ_e) decreases to 4.85 dB, resulting in a reduced relative error of 6.17%. Finally, at 1600 m, the RMSE rises to nearly 9 dBμV/m and the relative error exceeds 39%, accompanied by substantial overestimation (bias = 4.18 dB).

This behaviour, also evident in the MAE and nRMSE plots, highlights how empirical models like ITU-R P.1546-6 are influenced by terrain resolution in complex ways. Since this model incorporates terrain statistically rather than geometrically, resolution-dependent terrain smoothing may inadvertently reduce signal variance. This can sometimes lead to apparently improved relative errors, as observed at 800 m, but these improvements may stem from consistent overestimation rather than true accuracy. Overall, while the model tolerates mild resolution coarsening, it becomes increasingly unreliable in highly generalised terrain scenarios, both in terms of amplitude accuracy and predictive stability.

The PEM model displays significantly higher error levels than the ITU-R models across all terrain resolutions. Even at 100 m, the RMSE exceeds 11 dBμV/m and the relative error approaches 95%, indicating substantial discrepancies despite the fine spatial input. As the resolution coarsens, the error metrics deteriorate rapidly. At 400 m, the RMSE doubles to 20.8 dBμV/m, and the relative error exceeds 800%. At 1600 m, the RMSE reaches 36.4 dBμV/m, while the relative error exceeds 2200%. These extreme values suggest that the PEM implementation in this study—designed primarily for terrain-guided propagation—does not handle coarse elevation data gracefully. The model likely overfits to fine terrain details, and the lack of such information at coarse resolutions disrupts the ray curvature and ducting estimations that PEM relies on. Among all the models evaluated, PEM is by far the most sensitive to terrain generalization, as clearly illustrated in Fig. 9, which shows a line-based calculation between the test base station and a test point using both 50 m and 1600 m terrain resolutions.

It is clearly observable that thinning the terrain profile and subsequently filling the gaps using linear interpolation can easily result in the loss of narrow but significant obstacles in the landscape. In the case of a model with high terrain sensitivity, such as PEM, this can result in substantial errors. In this particular example, the test point lies just behind such an obstacle; therefore, when using a high-resolution terrain profile, the calculated field strength is very low, around −52 dBμV/m. However, when the terrain profile is downsampled to a 1600 m resolution, the obstructing effect of the terrain feature is lost.

Due to interpolation, the end of the profile coincides with the top of the obstacle, which leads to the opposite effect: instead of being shadowed by the obstruction, the receiver appears to be positioned on top of it, benefiting from improved line-of-sight conditions. This results in a significantly higher field strength of approximately 46 dBμV/m. This example clearly explains the extreme errors observed and highlights that PEM is considerably more sensitive to terrain characteristics as an input parameter than the other models.

In urban, hilly environments, the ITU-R P.1812-6 model demonstrates excellent predictive accuracy when high-resolution terrain data are used. At 100 m and 200 m terrain sampling intervals, the model achieves mean absolute error

and root mean square error values below 1.3 dBµV/m, with relative errors remaining under 8.5%. These results indicate that, at finer spatial resolutions, the model is able to account for terrain-induced diffraction effects with a high degree of reliability.

However, this performance advantage deteriorates rapidly as the terrain resolution becomes coarser. At 400 m and 800 m resolutions, RMSE values exceed 5 dBµV/m and relative errors rise sharply, surpassing 34%. At 1600 m resolution, the model's predictive accuracy breaks down entirely, with relative errors exceeding 220%, reflecting a drastic misrepresentation of the actual propagation environment.

This pronounced degradation highlights the model's strong dependency on detailed terrain input. As spatial detail is lost, the diffraction mechanisms that the model attempts to simulate become increasingly disconnected from the true physical conditions, resulting in significant overestimation or underestimation of field strength.

While the overall trend bears some resemblance to that of the ITU-R P.452-16 model at lower resolutions, P.1812-6 consistently produces slightly higher relative errors across all scales. This distinction is clearly supported by the plotted error metrics and should be taken into account when selecting models for simulations involving generalised or low-resolution terrain data.

In summary, the evaluation of different propagation models under varying terrain resolutions in an urban, hilly environment highlights the critical importance of spatial detail in accurate field strength prediction. While the ITU-R P.452-16 and P.1812-6 models perform reliably at high-resolution terrain inputs, their accuracy diminishes markedly with coarser raster data.

The ITU-R P.1546-6 model, though more tolerant to terrain simplification, still exhibits non-linear behaviour as generalisation increases. By contrast, the PEM model shows extreme sensitivity to resolution loss, with prediction errors escalating rapidly even at moderate levels of generalisation.

The visual comparison of field strength maps in Fig. 10 further supports these conclusions, revealing how each model's spatial prediction fidelity deteriorates as terrain resolution coarsens.

4.2 Flat Terrain

Before having precise knowledge of the test point-based results obtained over flat, lowland terrain, it is reasonable to assume that in such cases, reducing the resolution of terrain data has a significantly smaller impact on the accuracy of the simulated field strength levels. This is due to the fact that the terrain profile contains far fewer abrupt changes and prominent topographical features. Consequently, if the terrain is known to be flat, it may be possible to reduce the sampling density, which can lead to lower computational demands and faster simulation results.

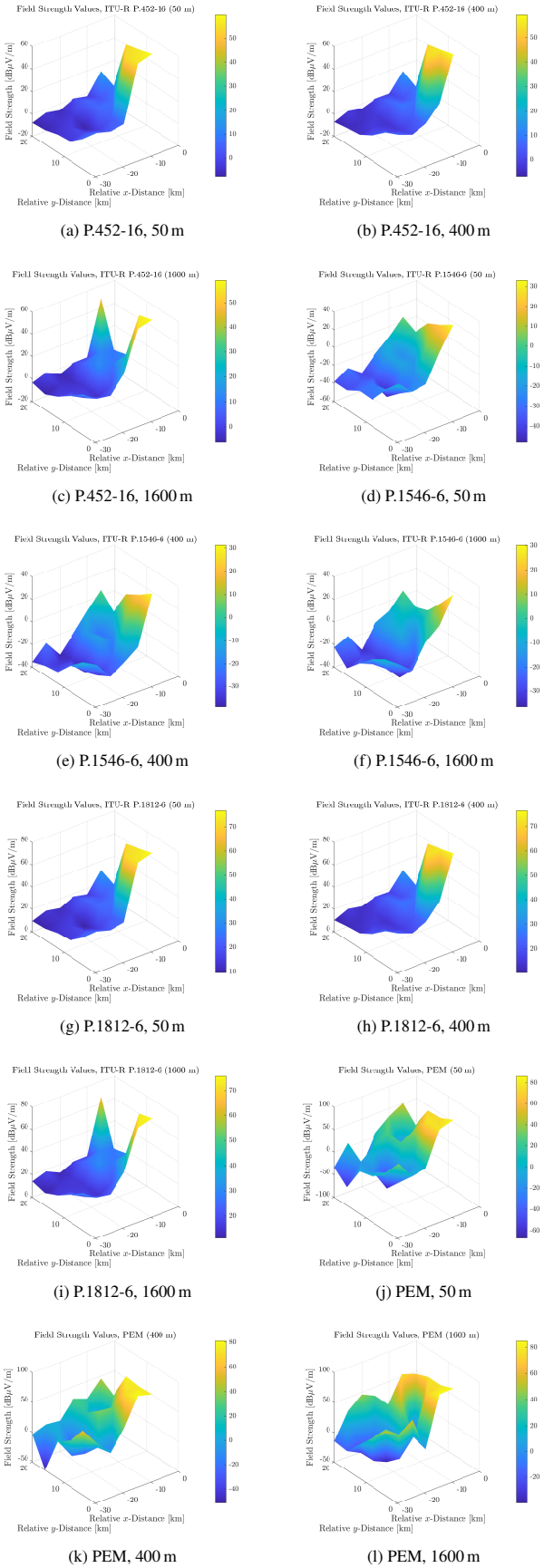

(a) P.452-16, 50 m (b) P.452-16, 400 m

(c) P.452-16, 1600 m (d) P.1546-6, 50 m

(e) P.1546-6, 400 m (f) P.1546-6, 1600 m

(g) P.1812-6, 50 m (h) P.1812-6, 400 m

(i) P.1812-6, 1600 m (j) PEM, 50 m

(k) PEM, 400 m (l) PEM, 1600 m

Fig. 10. Field strength maps for different raster resolutions (50 m, 400 m, 1600 m) across all models (ITU-R P.452-16, P.1546-6, P.1812-6, and PEM) in urban, hilly terrain.

The simulation results for flat terrain are presented in Tab. 5. The outcomes support the initial hypothesis, confirming that the simplicity of flat terrain significantly reduces the impact of sampling resolution reduction on the accuracy of field strength predictions. While in urban, hilly environments coarser terrain models introduced substantial errors already at 400–800 m raster resolutions, several models maintain relatively stable performance up to 800 m in flat areas.

The ITU-R P.452-16 model continues to provide accurate predictions over flat terrain at 100 m and 200 m raster resolutions: the errors remain small, and the relative error is around 6%. At 400 m, the errors increase noticeably, but not dramatically. In contrast, at 800 m and 1600 m resolutions, a sharp degradation in accuracy is observed, with the relative error exceeding 50%, which aligns well with the observation that this model is particularly sensitive to the loss of terrain detail, regardless of whether the environment is flat or hilly.

In the case of the ITU-R P.1812-6 model, the error trends are nearly identical to those of the ITU-R P.452-16 model, especially in the 100–400 m resolution range. In these cases, the RMSE remains below 1.2 dB, and the relative error is under 10.6%. This indicates that as long as the terrain remains homogeneous, the model is capable of accurately tracking propagation conditions. However, at 800 m and 1600 m resolutions, a rapid increase in error also appears here, indicating the model's sensitivity to terrain detail. Still, these deviations remain less severe than those observed in urban, hilly environments.

The parallel behavior of the error metrics with respect to raster resolution is evident not only in flat areas but also in the simulation results for complex terrain. It is important to emphasize, however, that the absolute predicted field strength levels differ between the two models; the similarity appears solely in the raster-dependent trends of the error metrics. This can also be observed in Fig. 11.

This similarity is not coincidental: both models are based on similar principles, particularly in the treatment of diffraction, ray-tracing, and anomalous propagation components. Nevertheless, the ITU-R P.1812-6 model relies on more detailed climate zones and statistical distributions and explicitly addresses the specific characteristics of the land mobile service, resulting in generally more conservative predictions. The similar dependence of the metrics on terrain resolution primarily stems from the fact that the mathematical treatment of terrain-related components is largely equivalent in both models, even though their practical scope and target services differ.

The performance of the ITU-R P.1546-6 model over flat terrain is particularly convincing. Within the 100–400 m resolution range, the RMSE consistently remains below 0.32 dB, while the relative error stays under 2.5%. These values are significantly more favourable than those observed in urban environments, where even at 400 m resolution, the RMSE exceeded 5 dB and the relative error approached 20%. Even at a raster resolution of 800 m, only moderate distortion is observed, indicating that the model tolerates resolution reduction well over flat terrain.

Test-point results: Flat terrain						
Resolution	**MAE** [dB]	**RMSE** [dB]	**Bias** [dB]	σ_e [dB]	**RelErr** [%]	**nRMSE** [–]
ITU-R P.452-16						
100 m	0.430	1.164	0.230	1.141	5.98	0.0312
200 m	0.540	0.845	0.093	0.840	6.34	0.0227
400 m	0.920	1.188	0.107	1.184	10.60	0.0319
800 m	2.577	4.628	1.910	4.215	52.76	0.1241
1600 m	3.497	4.841	0.670	4.795	59.64	0.1298
ITU-R P.1546-6						
100 m	0.057	0.091	–0.050	0.076	0.74	0.0022
200 m	0.120	0.181	–0.040	0.176	1.40	0.0044
400 m	0.213	0.314	0.200	0.242	2.46	0.0076
800 m	0.330	0.467	0.277	0.376	4.05	0.0113
1600 m	1.403	1.981	–1.323	1.475	16.87	0.0480
ITU-R P.1812-6						
100 m	0.430	1.164	0.230	1.141	5.98	0.0315
200 m	0.550	0.865	0.110	0.858	6.49	0.0234
400 m	0.920	1.192	0.127	1.185	10.65	0.0322
800 m	2.590	4.598	1.923	4.177	52.32	0.1243
1600 m	3.340	4.806	1.027	4.695	58.38	0.1299
PEM						
100 m	1.270	2.472	0.756	2.354	19.22	0.1040
200 m	1.431	2.177	0.856	2.001	19.74	0.0915
400 m	2.240	3.915	1.270	3.703	41.20	0.1646
800 m	3.375	5.579	1.383	5.405	80.37	0.2346
1600 m	6.006	7.723	0.599	7.700	107.33	0.3247

Tab. 5. Test point-based error metrics in flat environments.

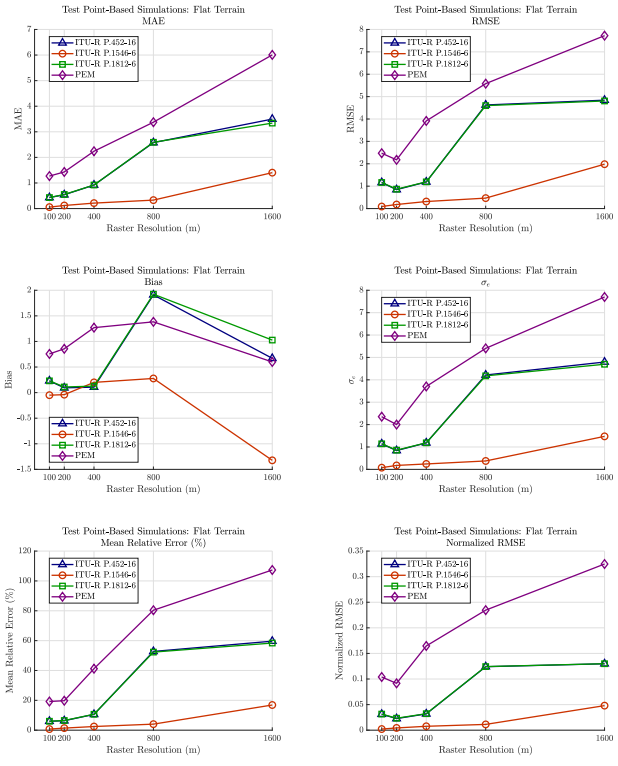

Fig. 11. Test point-based error metrics of simulations over flat terrain at varying terrain resolutions.

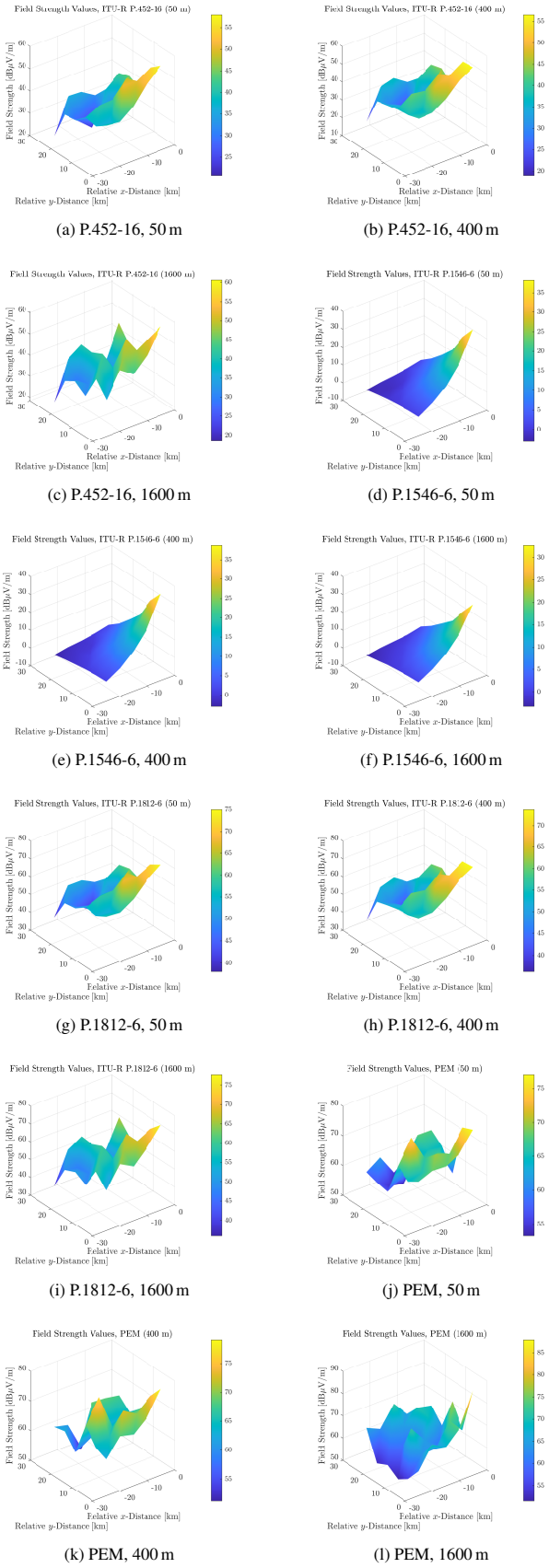

(a) P.452-16, 50 m (b) P.452-16, 400 m

(c) P.452-16, 1600 m (d) P.1546-6, 50 m

(e) P.1546-6, 400 m (f) P.1546-6, 1600 m

(g) P.1812-6, 50 m (h) P.1812-6, 400 m

(i) P.1812-6, 1600 m (j) PEM, 50 m

(k) PEM, 400 m (l) PEM, 1600 m

Fig. 12. Field strength maps for different raster resolutions (50 m, 400 m, 1600 m) across all models (ITU-R P.452-16, P.1546-6, P.1812-6, and PEM) in flat terrain.

In the case of the PEM model, the results over flat terrain also reflect the previously observed high sensitivity. Although the errors are somewhat lower than in hilly environments, the relative errors still exceed 19% even at a 100 m resolution, and rise above 107% at 1600 m. The field strength behavior at the examined test points across all four propagation models is presented in Fig. 12.

Overall, it can be stated that most models tolerate the reduction in sampling density better over flat terrain than under more varied topographical conditions. The ITU-R P.1546-6 model in particular demonstrates outstanding stability, while the ITU-R P.452-16 and ITU-R P.1812-6 models maintain acceptable error levels up to 400 m. The PEM model, however, continues to produce significant errors, and its application with generalised terrain data is therefore not recommended even in flat environments.

4.3 Mountainous Terrain

The mountainous terrain profile is characterized by rapid elevation changes over short horizontal distances, resulting in a highly fragmented topography. It is therefore reasonable to hypothesise that this terrain category would yield the highest numerical values across the evaluated error metrics. This expectation stems from the fact that when even a small proportion of elevation samples is removed and replaced with linearly interpolated values, the resulting terrain profile may fail to capture critical features such as ridges, valleys, and steep slopes. The simulation results, summarised in Tab. 6, provide clear confirmation of this assumption.

Test-point results: Mountainous terrain						
Resolution	**MAE** [dB]	**RMSE** [dB]	**Bias** [dB]	σ_e [dB]	**RelErr** [%]	**nRMSE** [–]
ITU-R P.452-16						
100 m	3.217	7.580	0.137	7.579	71.66	0.1170
200 m	4.963	9.823	–1.063	9.765	57.90	0.1516
400 m	6.710	12.983	4.177	12.292	740.12	0.2004
800 m	10.743	17.031	7.990	15.040	1700.7	0.2628
1600 m	13.890	20.521	13.777	15.209	1913.5	0.3167
ITU-R P.1546-6						
100 m	1.690	3.629	–0.283	3.618	17.58	0.0917
200 m	2.350	3.690	0.070	3.689	27.82	0.0932
400 m	2.610	4.568	1.397	4.349	48.31	0.1154
800 m	4.220	6.497	3.447	5.508	98.98	0.1641
1600 m	4.513	6.760	3.927	5.502	104.95	0.1707
ITU-R P.1812-6						
100 m	3.233	7.586	0.153	7.584	59.92	0.1174
200 m	4.963	9.805	–1.043	9.749	53.38	0.1518
400 m	6.717	12.952	4.150	12.270	609.02	0.2005
800 m	10.713	16.983	7.973	14.994	1440.7	0.2629
1600 m	13.817	20.409	13.710	15.119	2527.6	0.3159
PEM						
100 m	6.659	9.092	2.591	8.715	214.77	0.0500
200 m	12.092	17.034	2.949	16.776	333.21	0.0936
400 m	22.412	38.615	12.921	36.390	1690.5	0.2123
800 m	27.173	41.687	22.394	35.161	21349	0.2292
1600 m	25.632	39.733	18.648	35.086	18461	0.2185

Tab. 6. Test point-based error metrics in mountainous environments.

It is apparent that each metric yields quantitatively higher values by nearly an order of magnitude, which, without the need for further detailed analysis, clearly suggests that, in this case, the possibility of reducing terrain profile resolution without significantly compromising accuracy is extremely limited.

In the case of the ITU-R P.452-16 model, as also illustrated in Fig. 13, the increase in error metrics systematically follows the decrease in terrain resolution. The MAE rises from the initial value of 3.2 dB to 13.9 dB, while the RMSE more than doubles, increasing from 7.58 dB to 20.52 dB. The bias initially turns negative (–1.063 dB at 200 m resolution) and subsequently shifts to a markedly positive range (13.777 dB at 1600 m), indicating a consistent overestimation tendency at coarse resolutions. The relative error exhibits a dramatic increase, jumping from 71.7% to 1913.5%, which signals considerable instability. The nRMSE also increases from 0.1170 to 0.3167, confirming that this model is particularly sensitive to the loss of detailed topographic information.

The behaviour of the ITU-R P.1546-6 model is somewhat more balanced. The bias increases only slightly (from -0.283 dB to 3.927 dB) and remains within the positive domain throughout, indicating a mild overestimation tendency. The MAE and RMSE approximately double or slightly more, yet their absolute values remain moderate even at the coarsest resolution (MAE: 4.5 dB, RMSE: 6.76 dB). Although the relative error also increases markedly (from 17.58% to 104.95%), its magnitude remains substantially lower than that observed in the other models. The nRMSE increases from 0.0917 to 0.1707, suggesting a comparatively robust performance. The ITU-R P.1546-6 model maintains a more consistent error profile under reduced terrain resolution, highlighting its resilience in complex topographic conditions. However, all of this should be considered in the context that, despite its relative stability, the accuracy of this model remains considerably inferior when compared to the PEM [3].

The results of the ITU-R P.1812-6 model exhibit a pattern very similar to that of the ITU-R P.452-16 model, although the relative errors increase even more markedly. The relative error rises from 59.92% to as high as 2527.6%. The behavior of the bias closely mirrors that of ITU-R P.452-16: it starts at a slightly positive value, becomes negative at 200 m, and then increases sharply to 13.71 dB at 1600 m. The RMSE increases from 7.586 dB to 20.409 dB, while the normalized RMSE rises from 0.1174 to 0.3159. These results suggest that the ITU-R P.1812-6 model is particularly unstable in mountainous environments, especially in terms of relative error.

Figure 14 provides a visual representation of the spatial distribution of the resulting field strength levels. From the perspective of numerical error, the PEM model performs particularly poorly in this environment. Even at the finest resolution of 100 m, it produces the highest MAE (6.659 dB) and RMSE (9.092 dB) values among all models, and these figures deteriorate substantially with reduced resolution: the maximum MAE reaches 27.173 dB, while the RMSE climbs to 41.687 dB. The bias increases from 2.591 dB to 22.394 dB, indicating that underestimation is not characteristic, whereas overestimation becomes significantly pronounced. The relative errors are by far the most extreme among all models: starting at 214.77%, they rise to an astonishing 21 349%, and then stabilise at 18 461%. This indicates extreme instability and a high sensitivity to interpolated terrain data. The nRMSE also exceeds 0.21, which points to a breakdown of the model's reliability at coarse resolution levels.

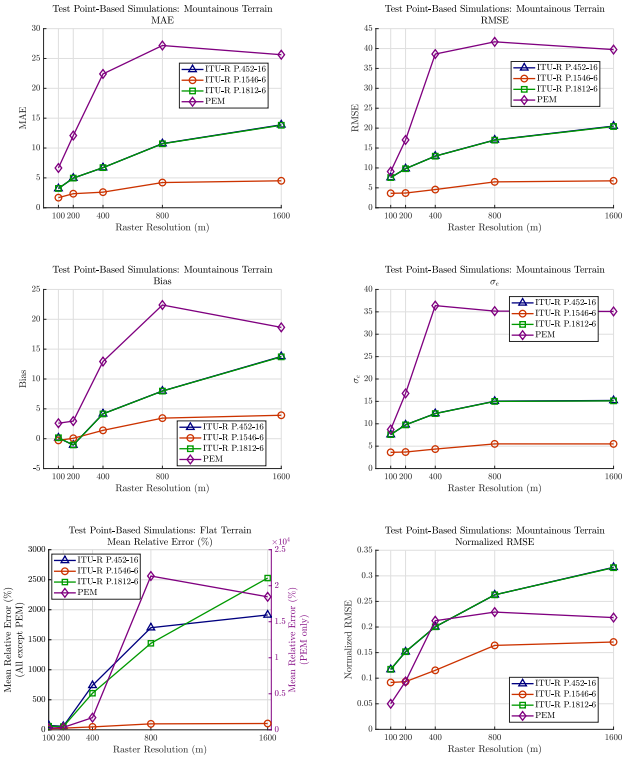

Fig. 13. Test point-based error metrics of simulations over mountainous terrain at varying terrain resolutions.

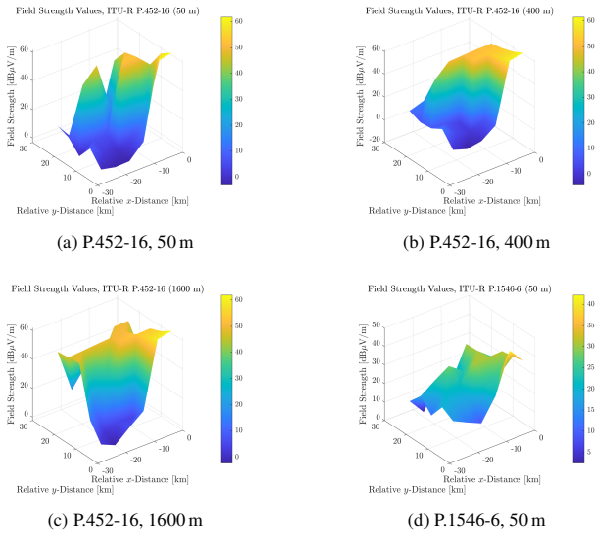

(a) P.452-16, 50 m (b) P.452-16, 400 m

(c) P.452-16, 1600 m (d) P.1546-6, 50 m

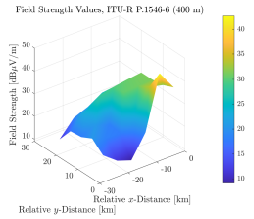

(e) P.1546-6, 400 m

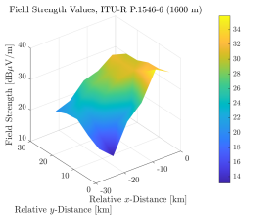

(f) P.1546-6, 1600 m

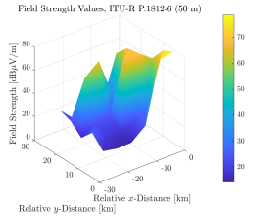

(g) P.1812-6, 50 m

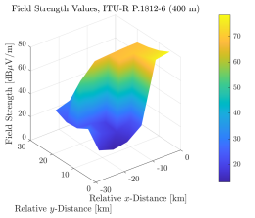

(h) P.1812-6, 400 m

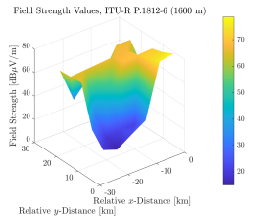

(i) P.1812-6, 1600 m

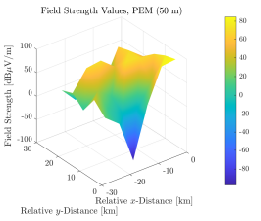

(j) PEM, 50 m

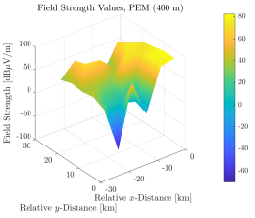

(k) PEM, 400 m

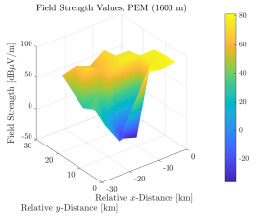

(l) PEM, 1600 m

Fig. 14. Field strength maps for different raster resolutions (50 m, 400 m, 1600 m) across all models (ITU-R P.452-16, P.1546-6, P.1812-6, and PEM) in mountainous terrain.

5. Line-Based Results

For the line-based calculations, 200 segments of 30 km length are randomly selected for each of the three terrain types, and the simulations are carried out on these segments and their corresponding terrain profiles at all terrain resolutions. In addition to the descriptive metrics, the spectral resolution of the terrain profiles is also considered here, along with the relationship between the spectral complexity ratio and the RMSE.

5.1 Urban, Hilly Terrain

Based on Tab. 7 and Fig. 15, it is evident that in urban, hilly terrain the line-based evaluation produced consistently higher errors for all models compared to the test point–based approach.

Line-Based Results: Urban, Hilly Terrain						
Resolution	**MAE** [dB]	**RMSE** [dB]	**Bias** [dB]	σ_e [dB]	**RelErr** [%]	**nRMSE** [–]
ITU-R P.452-16						
100 m	0.933	2.606	0.562	2.545	18.57	0.0220
200 m	2.021	4.428	1.459	4.180	55.66	0.0374
400 m	3.502	6.635	2.857	5.989	138.33	0.0561
800 m	5.838	9.746	5.121	8.292	349.94	0.0823
1600 m	9.710	14.651	9.005	11.557	1099.8	0.1238
ITU-R P.1546-6						
100 m	0.956	2.678	0.515	2.628	11.33	0.0149
200 m	1.910	4.226	1.274	4.029	25.62	0.0235
400 m	3.129	5.911	2.396	5.403	46.77	0.0329
800 m	4.682	7.844	3.814	6.854	78.61	0.0436
1600 m	6.756	10.194	5.775	8.400	134.03	0.0567
ITU-R P.1812-6						
100 m	0.904	2.556	0.544	2.497	17.97	0.0216
200 m	1.958	4.347	1.411	4.111	53.96	0.0367
400 m	3.402	6.521	2.772	5.902	134.24	0.0551
800 m	5.660	9.554	4.948	8.173	333.69	0.0807
1600 m	9.431	14.372	8.715	11.429	1034.3	0.1214
PEM						
100 m	6.635	10.163	2.000	9.965	100.6	0.0243
200 m	10.930	16.274	5.154	15.436	395.9	0.0389
400 m	14.773	21.472	9.632	19.191	1391.5	0.0513
800 m	20.180	28.963	15.727	24.321	3993.4	0.0691
1600 m	28.111	39.034	24.779	30.161	13443	0.0932

Tab. 7. Line-based error metrics in urban, hilly environments.

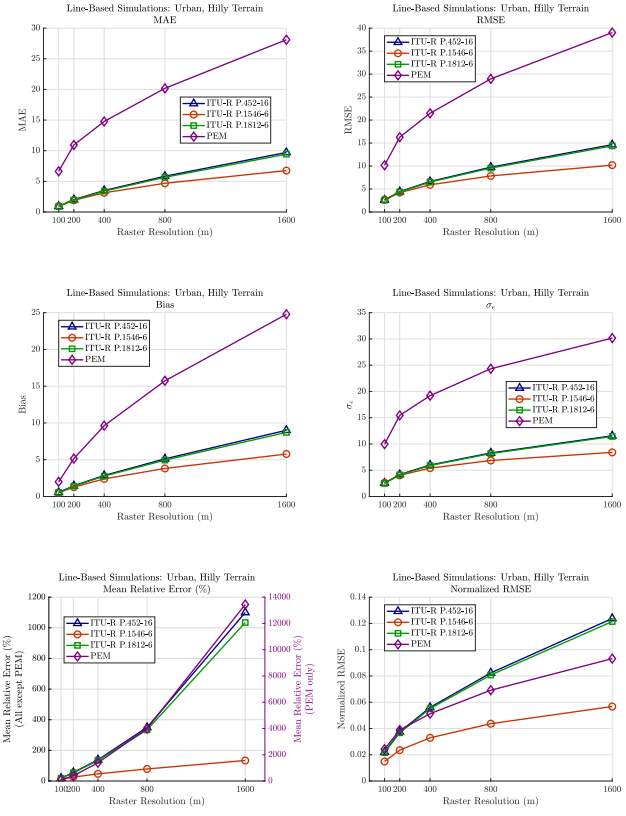

Fig. 15. Line-based error metrics of simulations over urban, hilly terrain at varying terrain resolutions.

The most striking difference can be observed for ITU-R P.452-16 and ITU-R P.1812-6, which not only yield similar error magnitudes but also track each other almost identically across all resolutions. With the test point reference, both models produced RMSE values close to 1 dB at 100–200 m resolution, while under the line-based reference these values rose to around 2–4 dB.

This demonstrates that line-based reference more sensitively exposes distortions caused by raster thinning, and that both models are equally more vulnerable to resolution degradation in this environment.

By contrast, ITU-R P.1546-6 shows a more balanced behavior. Even with test point comparisons it exhibited somewhat higher errors than P.452-16 or P.1812-6, yet when evaluated against the line-based reference, its performance deteriorated much less severely.

For example, at 1600 m resolution the RMSE increased by only about 1 dB (from 9 dB to 10 dB), whereas the other two models showed jumps of 2–3 dB. This clearly indicates that in urban, hilly terrain ITU-R P.1546-6 is less sensitive to changes in raster density and thus provides a more stable choice when the input data resolution cannot be guaranteed.

The deterministic PEM model, however, performed substantially worse under both references, with the differences being even more pronounced. While at 100 m resolution the RMSE already exceeded 11 dB with the test point evaluation, under the line-based calculations it increased to nearly 39 dB at 1600 m, and the relative errors reached several orders of magnitude higher than those of the ITU-R models. This clearly highlights that PEM is far more sensitive to raster thinning than the empirical models, and in urban, hilly terrain the choice of reference resolution becomes a critical factor for obtaining reliable results.

The regression parameters in Tab. 8 and the trends illustrated in Fig. 16 show that the error metrics of all evaluated models are strongly dependent on the spectral complexity of the terrain profiles. For the ITU-R P.452-16 and P.1812-6 models, the linear regressions already produced high explanatory power (the coefficient of determination $R^2 \approx 0.87$), but the exponential fits further improved the performance to $R^2 \approx 0.97$. This indicates that in these models the increase of RMSE with spectral complexity is systematic and very well captured by a saturating nonlinear function. The close similarity between the two models also confirms their parallel behavior observed earlier in direct error comparisons.

The ITU-R P.1546-6 model displayed weaker correlations than P.452-16 and P.1812-6. Its linear regression explained about 76% of the RMSE variance, while the exponential form increased this to around 95%. Although the fit quality is slightly lower than in the other ITU-R models, the results still highlight a consistent dependence between terrain spectral complexity and model errors. Interestingly, this model requires relatively higher values of parameter B, suggesting a steeper saturation effect compared to the other ITU-R recommendations.

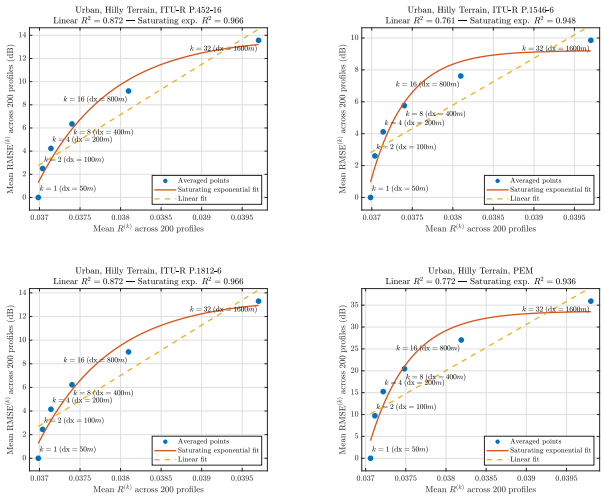

Fig. 16. Results of aggregated regression models for the different models over urban, hilly terrain.

Model	Type	Parameters	R^2
ITU-R P.452-16	Linear	$\beta_0 = -157.66,\ \beta_1 = 4337.25$	0.87
	Exp.	$c = 1.28,\ A = 12.54,\ B = 3.00$	0.97
ITU-R P.1546-6	Linear	$\beta_0 = -105.79,\ \beta_1 = 2936.42$	0.76
	Exp.	$c = 0.97,\ A = 8.24,\ B = 6.06$	0.95
ITU-R P.1812-6	Linear	$\beta_0 = -154.60,\ \beta_1 = 4252.91$	0.87
	Exp.	$c = 1.26,\ A = 12.30,\ B = 3.00$	0.97
PEM	Linear	$\beta_0 = -380.65,\ \beta_1 = 10544.73$	0.77
	Exp.	$c = 4.02,\ A = 29.60,\ B = 5.54$	0.94

Tab. 8. Regression results between spectral complexity ratio and RMSE for the evaluated models over urban, hilly terrain.

For the deterministic PEM model the regressions also revealed clear dependencies. The linear regression produced $R^2 \approx 0.77$, and the exponential fit improved this to about 0.94. Although the explained variance is somewhat lower than in the ITU-R models, the strength of the relationship remains substantial. The higher parameter values obtained for the PEM model indicate stronger sensitivity to terrain spectral content, which is consistent with its numerical nature and the large error growth already observed at coarse resolutions. Altogether, the regression analysis confirms that terrain spectral descriptors provide a reliable basis for interpreting the resolution sensitivity of propagation models.

5.2 Flat Terrain

The comparison of Tab. 9 and Tab. 7 reveals substantial differences between flat and urban, hilly terrain in line-based simulations. In flat environments, the growth of the error metrics with coarser terrain resolution is moderate and remains within a relatively narrow range, especially for the ITU-R P.1546-6 model, which shows RMSE values below 5 dB even at 1600 m resolution. By contrast, in urban, hilly terrain, all models exhibit a much steeper error growth, with RMSE values exceeding 10 dB at 1600 m resolution for the ITU-R P.452-16 and P.1812-6 models, and reaching nearly 40 dB for PEM. This indicates that spectral complexity and relief variations of the terrain are decisive factors for error amplification in the line-based approach.

Line-based results: Flat terrain						
Resolution	**MAE** [dB]	**RMSE** [dB]	**Bias** [dB]	σ_e [dB]	**RelErr** [%]	**nRMSE** [–]
ITU-R P.452-16						
100 m	1.770	3.568	1.307	3.319	33.61	0.0393
200 m	3.374	5.613	2.817	4.855	81.24	0.0618
400 m	5.080	7.681	4.577	6.168	154.34	0.0846
800 m	6.819	9.609	6.418	7.152	240.69	0.1059
1600 m	8.321	11.173	8.022	7.778	329.30	0.1231
ITU-R P.1546-6						
100 m	0.623	2.262	0.486	2.209	7.90	0.0166
200 m	1.053	3.224	0.932	3.087	14.60	0.0237
400 m	1.341	3.826	1.258	3.613	20.97	0.0281
800 m	1.512	4.090	1.416	3.837	24.73	0.0300
1600 m	1.610	4.167	1.453	3.905	26.32	0.0306
ITU-R P.1812-6						
100 m	1.733	3.494	1.261	3.259	32.51	0.0366
200 m	3.291	5.482	2.710	4.765	77.72	0.0575
400 m	4.947	7.492	4.405	6.061	146.68	0.0785
800 m	6.657	9.394	6.206	7.052	228.98	0.0985
1600 m	8.128	10.922	7.772	7.675	312.39	0.1145
PEM						
100 m	3.310	5.321	1.302	5.160	67.19	0.0373
200 m	5.160	7.699	2.662	7.224	181.91	0.0539
400 m	6.701	9.667	4.255	8.680	352.52	0.0677
800 m	8.047	11.281	5.644	9.768	539.89	0.0790
1600 m	8.903	12.391	6.727	10.406	750.97	0.0868

Tab. 9. Line-based error metrics in flat environments.

The relative behavior of the models is also consistent across environments but with significant differences in scale. In both terrains, ITU-R P.1546-6 proves to be the most robust, producing the lowest errors and the slowest degradation with increasing resolution. ITU-R P.452-16 and ITU-R P.1812-6 follow nearly identical patterns, confirming their parallel evolution observed earlier, but the absolute errors are considerably larger in hilly terrain. PEM, while already more sensitive in flat terrain than the ITU-R models, shows dramatically higher error values in the urban, hilly case, highlighting its strong dependence on terrain resolution and spectral complexity. These tendencies are also clearly reflected in Fig. 17, where the graphical representation of the error growth emphasizes the contrasting slopes across the different models and terrains.

A further contrast emerges when comparing line-based flat terrain results (Tab. 9) with the corresponding test point-based outcomes (Tab. 5). In the test point approach, the errors remain significantly lower across all models and resolutions. For example, in ITU-R P.452-16 at 800 m resolution, the line-based RMSE is 9.6 dB compared to only 4.6 dB in the test point evaluation. Similarly, for PEM at 1600 m resolution, the RMSE reaches 12.4 dB in line-based analysis, while it is as high as 7.7 dB in the test point-based case, confirming that line-based aggregation systematically produces larger errors by amplifying the effect of unresolved terrain fluctuations. Overall, these results demonstrate that while flat terrain leads to lower absolute errors.

The regression results over flat terrain, summarized in Fig. 18 and Tab. 10, show a markedly stronger fit between spectral complexity and error growth than in urban, hilly terrain. The exponential models achieve extremely high explanatory power, with R^2 values of 0.98–0.99 across all models, indicating that the saturating error increase with growing spectral complexity is captured almost perfectly in flat environments. Even the linear regressions of ITU-R P.452-16 and P.1812-6 yield $R^2 \approx 0.90$, substantially higher than their urban, hilly counterparts, while PEM maintains an acceptable level at $R^2 = 0.80$. By contrast, ITU-R P.1546-6 shows weaker linear correlation ($R^2 = 0.64$), but this is fully compensated by the exponential fit, which again approaches unity.

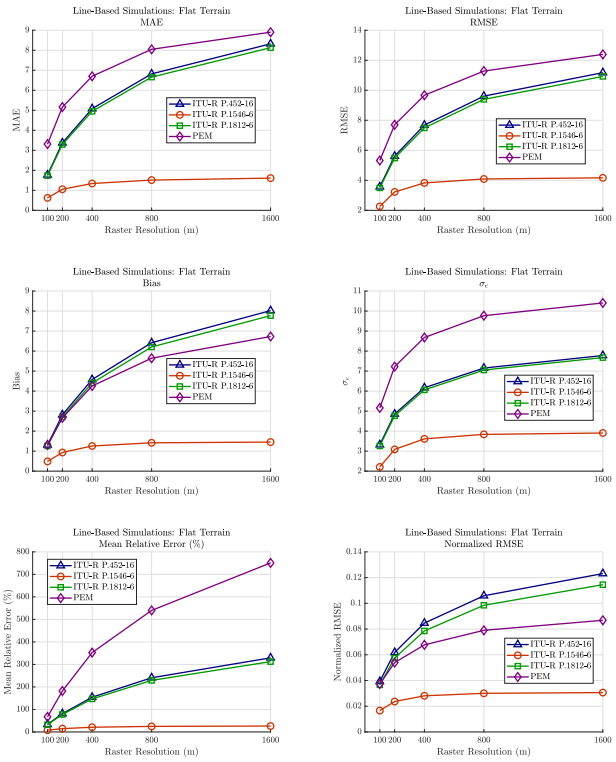

Fig. 17. Line-based error metrics of simulations over flat terrain at varying terrain resolutions.

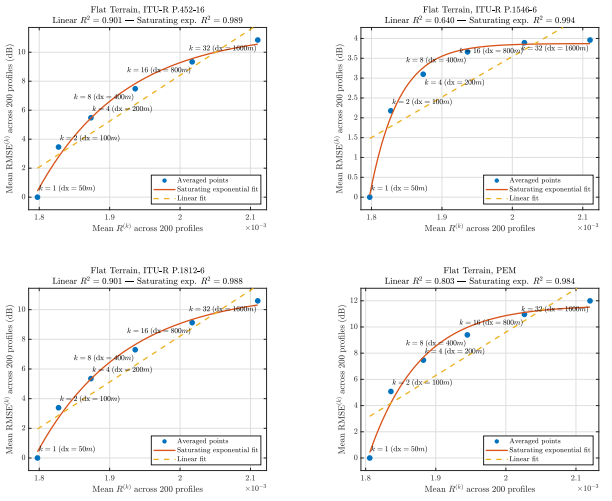

Fig. 18. Results of aggregated regression models for the different models over flat terrain.

Model	Type	Parameters	R^2
ITU-R P.452-16	Linear	$\beta_0 = -54.91,\ \beta_1 = 31663.02$	0.90
	Exp.	$c = 0.42,\ A = 11.03,\ B = 2.51$	0.99
ITU-R P.1546-6	Linear	$\beta_0 = -16.85,\ \beta_1 = 10196.25$	0.64
	Exp.	$c = 0.05,\ A = 3.82,\ B = 7.57$	0.99
ITU-R P.1812-6	Linear	$\beta_0 = -53.63,\ \beta_1 = 30924.70$	0.90
	Exp.	$c = 0.42,\ A = 10.78,\ B = 2.50$	0.99
PEM	Linear	$\beta_0 = -56.49,\ \beta_1 = 33046.35$	0.80
	Exp.	$c = 0.42,\ A = 11.26,\ B = 4.26$	0.98

Tab. 10. Regression results between spectral complexity ratio and RMSE for the evaluated models over flat terrain.

When compared with the urban, hilly results in Tab. 8, the differences in parameter magnitudes highlight the terrain sensitivity of the models. In hilly terrain, the intercepts c of the exponential models are higher (e.g., $c = 1.28$ for ITU-R P.452-16 and $c = 4.02$ for PEM) than in flat terrain ($c \approx 0.42$ across most models), reflecting the elevated baseline error induced by complex topography. Similarly, the slope coefficients β_1 of the linear models are one order of magnitude larger in flat terrain (e.g., $\beta_1 \approx 31663$ for P.452-16 vs. ≈ 4337 in hilly terrain), showing that once complexity increases, the error grows more steeply but from a much lower baseline. These results confirm that while the relative ranking of the models remains unchanged, so the ITU-R P.1546-6 being the most robust and PEM the most sensitive, the absolute error dynamics differ significantly between flat and hilly environments, with flat terrain yielding lower starting errors and tighter exponential saturation.

5.3 Mountainous Terrain

The line-based error metrics obtained for mountainous terrain are summarised in Tab. 11 and visualised in Fig. 19. Across all resolutions, the errors are considerably higher than in flat (Tab. 9) and urban, hilly terrain (Tab. 7), underlining the increased sensitivity of propagation models to rugged topography. ITU-R P.1546-6 continues to show the lowest error growth with resolution, with RMSE values rising from 3.5 dB at 100 m to 14.3 dB at 1600 m.

A comparison with the urban, hilly case reveals that although the relative ranking of models remains consistent across environments, the absolute magnitude of errors is greatly amplified in mountainous terrain. This amplification can be seen most clearly in the RMSE values: at 800 m resolution, ITU-R P.452-16 increases from 9.7 dB in the urban, hilly case to 12.9 dB in the mountainous scenario, while PEM rises from 29.0 dB to 44.8 dB. The escalation of errors is thus not limited to the deterministic PEM but also affects the empirical ITU-R models, albeit to a lesser extent. The bias and variance components follow the same tendency, with systematic deviations and random fluctuations both becoming more pronounced as terrain ruggedness increases.

Line-based results: Mountainous terrain						
Resolution	**MAE** [dB]	**RMSE** [dB]	**Bias** [dB]	σ_e [dB]	**RelErr** [%]	**nRMSE** [–]
ITU-R P.452-16						
100 m	1.063	2.775	0.619	2.705	21.51	0.0229
200 m	2.366	4.913	1.741	4.594	73.98	0.0405
400 m	4.488	8.070	3.788	7.125	262.51	0.0665
800 m	8.068	12.887	7.408	10.545	955.91	0.1062
1600 m	13.251	19.203	12.781	14.332	3158	0.1583
ITU-R P.1546-6						
100 m	1.316	3.515	0.655	3.453	15.59	0.0185
200 m	2.668	5.582	1.750	5.300	38.72	0.0293
400 m	4.644	8.205	3.581	7.382	82.83	0.0431
800 m	7.183	11.133	6.073	9.331	161.14	0.0585
1600 m	9.974	14.259	8.828	11.198	320.83	0.0750
ITU-R P.1812-6						
100 m	1.031	2.719	0.599	2.652	20.87	0.0220
200 m	2.288	4.804	1.683	4.500	71.21	0.0389
400 m	4.344	7.900	3.661	7.001	250.57	0.0640
800 m	7.806	12.614	7.158	10.386	899.87	0.1021
1600 m	12.830	18.791	12.356	14.157	2895.8	0.1521
PEM						
100 m	12.522	17.848	4.072	17.377	455.84	0.0400
200 m	18.562	26.280	9.635	24.450	1358.2	0.0590
400 m	25.285	34.973	18.635	29.594	5068.4	0.0785
800 m	33.401	44.831	27.214	35.625	16893	0.1006
1600 m	43.877	56.798	38.365	41.883	40515	0.1274

Tab. 11. Line-based error metrics in mountainous environments.

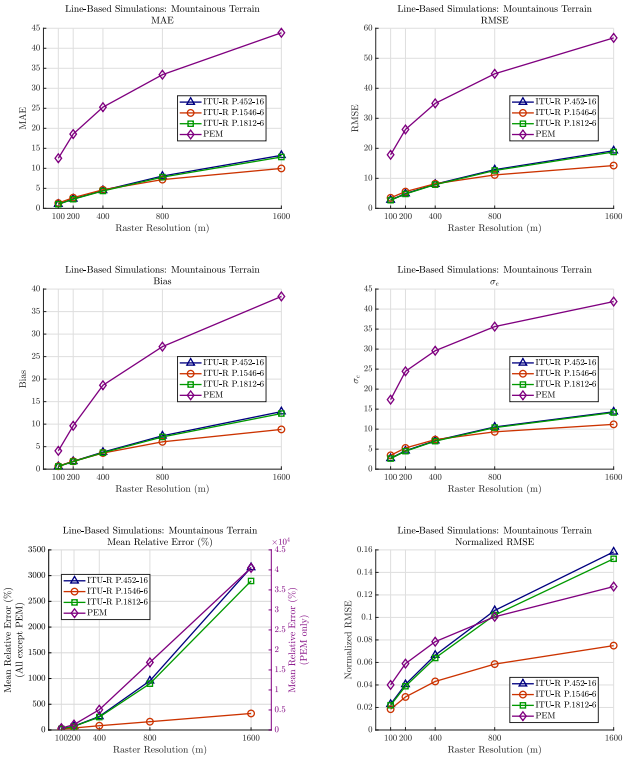

Fig. 19. Line-based error metrics of simulations over mountainous terrain at varying terrain resolutions.

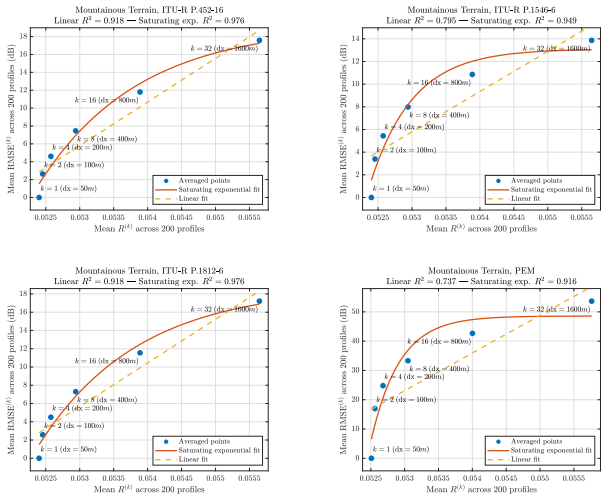

Fig. 20. Results of aggregated regression models for the different models over mountainous terrain.

In addition to RMSE, other error metrics highlight the severity of the mountainous environment. For example, the mean relative error in linear field units climbs to several thousand percent for PEM, compared to only a few hundred percent for the ITU-R models at the coarsest resolutions. This widening gap reflects the fundamental differences in how the models account for terrain detail: ITU-R P.1546-6, while still affected, shows relatively moderate growth due to its reliance on empirical calibration, whereas PEM is particularly vulnerable to undersampling of complex topography. Taken together, these results clearly demonstrate the limits of deterministic approaches when terrain irregularities are insufficiently resolved, and they emphasise the critical importance of terrain resolution for maintaining model reliability in mountainous regions.

The regression analysis between spectral complexity ratio and RMSE (Fig. 20, Tab. 12) provides further insight into these behaviours. Linear models achieve R^2 values around 0.9 for ITU-R P.452-16 and P.1812-6, while ITU-R P.1546-6 reaches only 0.79, consistent with its smoother error progression. Saturating exponential regressions, however, consistently outperform linear fits, with R^2 values of 0.95–0.98 across the ITU-R models. This indicates that error growth with spectral complexity is nonlinear and tends to stabilise, a behaviour captured effectively by the exponential form.

Compared to flat and urban, hilly terrains, the regression slopes and asymptotic error levels are markedly higher in mountainous environments. For example, the exponential saturation level A reaches 17.7 dB for ITU-R P.452-16 and 42.0 dB for PEM, compared to 12.54 dB and 29.6 dB, respectively, in the urban, hilly case. These results emphasise the strong dependence of model accuracy on spectral complexity, with PEM particularly exposed to terrain ruggedness. The consistency of regression quality across all environments nonetheless confirms that spectral descriptors offer a reliable predictor of error escalation, irrespective of the propagation model considered.

Model	Type	Parameters	R^2
ITU-R P.452-16	Linear	$\beta_0 = -252.93,\ \beta_1 = 4881.60$	0.92
	Exp.	$c = 1.52,\ A = 17.69,\ B = 2.20$	0.98
ITU-R P.1546-6	Linear	$\beta_0 = -182.48,\ \beta_1 = 3552.33$	0.79
	Exp.	$c = 1.52,\ A = 11.59,\ B = 5.16$	0.95
ITU-R P.1812-6	Linear	$\beta_0 = -247.66,\ \beta_1 = 4779.70$	0.92
	Exp.	$c = 1.48,\ A = 17.32,\ B = 2.20$	0.98
PEM	Linear	$\beta_0 = -659.37,\ \beta_1 = 12876.16$	0.74
	Exp.	$c = 6.54,\ A = 42.04,\ B = 7.71$	0.92

Tab. 12. Regression results between spectral complexity ratio and RMSE for the evaluated models over mountainous terrain.

The line-based simulations extend and refine the findings obtained from the test-point-based analyses. While the test-point simulations provided a discrete, location-specific evaluation of the model sensitivity to terrain sampling density, the line-based computations offered a much denser sampling along the entire propagation path, resulting in a more accurate and statistically robust characterization of the models' behavior. The larger number of calculated points enables a smoother depiction of the trend between terrain resolution and propagation error, confirming the general tendencies observed in the test-point-based approach. Furthermore, the line-based analysis introduces the concept of the spectral complexity ratio, which establishes a quantitative relationship between terrain characteristics and the average RMSE. This continuous evaluation framework thus provides deeper insight into the spatial evolution of modeling errors and strengthens the consistency and interpretability of the obtained results across different terrain types.

6. Conclusion

This study examined how terrain sampling density influences the accuracy of several widely used propagation models for 5G NR-V2X communication at 3.6 GHz. By testing empirical, hybrid, and deterministic models across flat, hilly, and mountainous environments, we showed that model sensitivity to terrain resolution strongly depends on both the modeling approach and the complexity of the environment. Empirical models proved relatively robust even at coarser resolutions, while deterministic and hybrid approaches performed very well with fine-grained inputs but degraded much more rapidly as resolution decreased.

A key scientific contribution of this work is the demonstrated link between the spectral complexity of terrain profiles and the resulting modeling error. By defining the spectral complexity ratio and relating it to RMSE through regression analysis, we showed that error growth can be predicted directly from terrain spectral characteristics. Exponential models achieved explanatory power close to 99%, proving that spectral descriptors serve as reliable predictors of model sensitivity. This provides a practical way to anticipate accuracy losses before simulations are carried out, which can make network planning more efficient and better informed.

The results also highlight the trade-off between computational demand and predictive fidelity, pointing to conditions where terrain simplification can be applied without major reliability risks. At the same time, the findings expose the limitations of purely deterministic approaches in complex topographies, while showing where empirical and hybrid models can offer more stable results.

Overall, the study underlines that terrain resolution is not a secondary detail, but a key factor in obtaining trustworthy propagation predictions. The proposed framework offers a methodological advance for adaptive and resource-efficient modeling, and it opens opportunities for further research such as applying the method to higher frequency bands, experimenting with alternative simplification techniques, or integrating machine learning into hybrid modeling approaches.

In the next phase of our research, we aim to further extend the presented analysis by developing artificial intelligence (AI)-based regression models that can approximate the results of PEM – which is known for its high accuracy but considerable computational cost – using the significantly faster and less complex empirical and hybrid ITU propagation models. These AI-driven approaches will be trained under specific constraints to reproduce PEM-level precision while maintaining computational efficiency. Future work will also include a comparative performance evaluation of the proposed regression models and the development of a measurement-based predictive model capable of estimating field strength levels directly from real-world observations using AI techniques.

In conclusion, this research provides a robust methodological foundation for terrain-aware propagation modeling and sets the stage for the development of AI-based regression frameworks that combine accuracy with computational efficiency. The outcomes are expected to support more adaptive, data-driven network planning across diverse environments. All MATLAB and Python codes developed during this research, along with the simulation source files and auxiliary scripts, are available from the corresponding author upon reasonable request.

Acknowledgments

The author, Tamás István Unger gratefully acknowledges the support of the National Media and Infocommunications Authority of Hungary (NMHH), whose provision of a calm and supportive institutional environment significantly contributed to the successful completion of his doctoral research. The availability of key software tools offered by the Authority further facilitated the technical preparation of this work. He extends his sincere appreciation to Irén Bálint, Head of Unit, whose thoughtful leadership and consistent encouragement cultivated a professional atmosphere defined by intellectual freedom and composure. He is also deeply indebted to Péter Vári, Deputy Director General of NMHH, for his steadfast support and enduring commitment to the author's academic pursuits since their inception. Furthermore, the author wishes to thank Széchenyi István University and the Doctoral School of Multidisciplinary Engineering Sciences (MMTDI) for their continued academic guidance and for fostering a research-oriented environment throughout the course of his doctoral studies.

References

[1] CÁTEDRA, M., PÉREZ-ARRIAGA, J. *Cell Planning for Wireless Communications*. 1st ed. Norwood (USA): Artech House, 1999. ISBN: 978-0-89006-945-9

[2] RAPPAPORT, T. S. *Wireless Communications: Principles and Practice*. 2nd ed. Upper Saddle River (USA): Prentice Hall, 2001. ISBN: 978-0130422323

[3] UNGER, T. I., KUCZMANN, M. Comparison of outdoor radiowave propagation models for land mobile systems in the 3.6 GHz and 6 GHz frequency bands. *Telecom*, 2025, vol. 6, no. 2, p. 1–41. DOI: 10.3390/telecom6020042

[4] CAMA-PINTO, D., DAMAS, M., HOLGADO-TERRIZA, J. A., et al. Empirical model of radio wave propagation in the presence of vegetation inside greenhouses using regularized regressions. *Sensors*, 2020, vol. 20, no. 22, p. 6621–6636. DOI: 10.3390/s20226621

[5] HAROUNABADI, M., SOLEYMANI, D. M., BHADAURIA, S., et al. V2X in 3GPP standardization: NR sidelink in Release-16 and beyond. *IEEE Communications Standards Magazine*, 2021, vol. 5, no. 1, p. 12–21. DOI: 10.1109/MCOMSTD.001.2000070

[6] AL HARTHI, F. R. A., TOUZENE, A., ALZIDI, N., et al. Intelligent handover decision-making for vehicle-to-everything (V2X) 5G networks. *Telecom*, 2025, vol. 6, no. 3, p. 1–27. DOI: 10.3390/telecom6030047

[7] WAQAS, S. M., TANG, Y., YU, L., ABBAS, F. A joint cluster-based RRM and low-latency framework using the full-duplex mechanism for NR-V2X networks. *Computer Communications*, 2023, vol. 209, p. 513–525. DOI: 10.1016/j.comcom.2023.07.032

[8] TARIQ, S., AL-RIZZO, H., HASAN, M. N., et al. Stochastic versus ray tracing wireless channel modeling for 5G and V2X applications: opportunities and challenges. *Antenna Systems*, 2021, p. 1–16. DOI: 10.5772/intechopen.101625

[9] LI, J., TAYLOR, G., KIDNER, D. B. Accuracy and reliability of map-matched GPS coordinates: The dependence on terrain model resolution and interpolation algorithm. *Computers & Geosciences*, 2005, vol. 31, no. 2, p. 241–251. DOI: 10.1016/j.cageo.2004.06.011

[10] EUROPEAN COMMISSION. *Commission Implementing Decision 2014/276/EU of 2 May 2014 Amending Decision 2008/411/EC on the Harmonisation of the 3400–3800 MHz Frequency Band for Terrestrial Systems Capable of Providing Electronic Communications Services in the Community*. [Online] Cited 2025-07-21. Available at: https://eur-lex.europa.eu/eli/dec_impl/2014/276/oj

[11] ELECTRONIC COMMUNICATIONS COMMITTEE (ECC). *ECC Decision (11)06 of 9 December 2011 on Harmonised Frequency Arrangements for Mobile/Fixed Communications Networks (MFCN) Operating in the Band 3400–3800 MHz*. [Online] Cited 2025-07-21. Available at: https://docdb.cept.org/document/433

[12] RADIOCOMMUNICATION SECTOR OF INTERNATIONAL TELECOMMUNICATION UNION (ITU-R). *Radio Regulations 2024*. [Online] Cited 2025-07-21. Available at: http://handle.itu.int/11.1002/pub/8229633e-en

[13] ELECTRONIC COMMUNICATIONS COMMITTEE (ECC) WITHIN THE EUROPEAN CONFERENCE OF POSTAL AND TELECOMMUNICATIONS ADMINISTRATIONS (CEPT). *The European Table of Frequency Allocations in the Frequency Range 8.3 kHz to 3000 GHz (ECA Table) Approved January 2025*. [Online] Cited 2025-02-06. Available at: https://efis.cept.org/sitecontent.jsp?sitecontent=ecatable

[14] LUSVARGHI, L., MERANI, M. L. MoreV2X – A new radio vehicular communication module for ns-3. In *Proceedings of the 2021 IEEE 94th Vehicular Technology Conference (VTC2021-Fall)*. Norman (OK, USA), 2021, p. 1–7. DOI: 10.1109/VTC2021-Fall52928.2021.9625478

[15] ZHAO, Y., YANG, C., JI, T. Propagation characteristics of 3.6 GHz typical application scenarios based on parabolic equation [in Chinese]. *Dianbo Kexue Xuebao / Chinese Journal of Radio Science*, 2021, vol. 36, no. 4, p. 604–610. DOI: 10.12265/j.cjors.2020227

[16] AN, H., GUAN, K., WANG, X., et al. Vehicle-to-vehicle channel measurements and power domain modeling in mountainous plateau environments for emergency communications. *IEEE Transactions on Intelligent Transportation Systems*, 2024, vol. 25, no. 12, p. 21060–21073. DOI: 10.1109/TITS.2024.3465014

[17] YANG, C., WANG, J., YOU, X., et al. Applicability of ITU-R P.1546 recommendation in typical terrestrial areas of China [in Chinese]. *Dianbo Kexue Xuebao / Chinese Journal of Radio Science*, 2019, vol. 34, no. 3, p. 295–301. DOI: 10.13443/j.cjors.2018020801

[18] KALLIOVAARA, J., EKMAN, R., JOKELA, T., et al. Suitability of ITU-R P.1546 propagation predictions for allocating LTE SDL with GE06. In *Proceedings of the 2017 IEEE International Symposium on Broadband Multimedia Systems and Broadcasting (BMSB)*. Cagliari (Italy), 2017, p. 1–6. DOI: 10.1109/BMSB.2017.7986174

[19] ÖSTLIN, E., SUZUKI, H., ZEPERNICK, H.-J. Evaluation of the propagation model recommendation ITU-R P.1546 for mobile services in rural Australia. *IEEE Transactions on Vehicular Technology*, 2008, vol. 57, no. 1, p. 38–51. DOI: 10.1109/TVT.2007.901902

[20] LEVY, M. F. Parabolic equation modelling of propagation over irregular terrain. *Electronics Letters*, 1990, vol. 26, no. 15, p. 1153–1155. DOI: 10.1049/el:19900746

[21] DONOHUE, D. J., KUTTLER, J. R. Propagation modeling over terrain using the parabolic wave equation. *IEEE Transactions on Antennas and Propagation*, 2000, vol. 48, no. 2, p. 260–277. DOI: 10.1109/8.833076

[22] HOLM, P. D. Wide-angle shift-map PE for a piecewise linear terrain. In: *AIP Conference Proceedings*, 2009, vol. 1106, p. 56–65. DOI: 10.1063/1.3117113

[23] JANASWAMY, R. A Curvilinear coordinate-based split-step parabolic equation method for propagation predictions over terrain. *IEEE Transactions on Antennas and Propagation*, 1998, vol. 46, no. 7, p. 1089–1097. DOI: 10.1109/8.704813

[24] WEI, Q.-F., YIN, C.-Y., FAN, Q.-M. Research and verification for parabolic equation method of radio wave propagation in obstacle environment [in Chinese]. *Wuli Xuebao / Acta Physica Sinica*, 2017, vol. 66, no. 12, p. 1–7. DOI: 10.7498/aps.66.124102

[25] OCHI, G. M., SWEARINGEN, M. E. Parabolic equation comparisons with Galerkin discretization and boundary fitted grid for modeling infrasound propagation: 2D versus 3D. *Proceedings of Meetings on Acoustics*, 2021, vol. 45, no. 1, p. 1–13. DOI: 10.1121/2.0001551

[26] SILVA, M. A. N., COSTA, E., LINIGER, M. Analysis of the effects of irregular terrain on radio wave propagation based on a three-dimensional parabolic equation. *IEEE Transactions on Antennas and Propagation*, 2012, vol. 60, no. 4, p. 2138–2143. DOI: 10.1109/TAP.2012.2186227

[27] LI, J., WAGEN, J.-F., LACHAT, E. ITU model for multiknife-edge diffraction. *IEE Proceedings: Microwaves, Antennas and Propagation*, 1996, vol. 143, no. 6, p. 539–541. DOI: 10.1049/ip-map:19960884

[28] LU, J. S., HAN, X., BERTONI, H. L. The influence of terrain scattering on radio links in hilly/mountainous regions. *IEEE Transactions on Antennas and Propagation*, 2013, vol. 61, no. 3, p. 1385–1395. DOI: 10.1109/TAP.2012.2231919

[29] LI, X., WU, Z., WANG, S., JIAO, H. Path loss and blockage modeling for vehicle-to-vehicle channel above 6 GHz. In *Proceedings of the 2018 IEEE 4th International Conference on Computer and Communications (ICCCC 2018)*. Chengdu (China), 2018, p. 494–499. DOI: 10.1109/CompComm.2018.8780963

[30] BOBAN, M., BARROS, J., TONGUZ, O. K. Geometry-based vehicle-to-vehicle channel modeling for large-scale simulation. *IEEE Transactions on Vehicular Technology*, 2014, vol. 63, no. 9, p. 4146–4164. DOI: 10.1109/TVT.2014.2317803

[31] GONG, Y., WANG, S., ZHANG, Y., et al. VANETs LTE-V performance evaluation using 3D geometry-stochastic channel model. In *Proceedings of the 18th COTA International Conference of Transportation Professionals (CICTP 2018): Intelligence, Connectivity, and Mobility*. Beijing (China), 2018, p. 2778–2787. DOI: 10.1061/9780784481523.276

[32] RADIOCOMMUNICATION SECTOR OF INTERNATIONAL TELECOMMUNICATION UNION (ITU-R). *Recommendation ITU-R P.1546-6: Method for Point-to-Area Predictions for Terrestrial Services in the Frequency Range 30 MHz to 4000 MHz*. [Online] Cited 2025-07-21. Available at: https://www.itu.int/rec/R-REC-P.1546-6-201908-I/en

[33] RASOOL, H. F., QURESHI, M. A., AZIZ, A., et al. A. An introduction to the parabolic equation method for electromagnetic wave propagation in tunnels. *COMPEL - The International Journal for Computation and Mathematics in Electrical and Electronic Engineering*, 2022, vol. 41, no. 5, p. 1313–1331. DOI: 10.1108/COMPEL-07-2021-0245

[34] CRANK, J., NICOLSON, P. A practical method for numerical evaluation of solutions of partial differential equations of the heat-conduction type. *Mathematical Proceedings of the Cambridge Philosophical Society*, 1947, vol. 43, no. 1, p. 50–67. DOI: 10.1017/S0305004100023197

[35] LEVY, M. *Parabolic Equation Methods for Electromagnetic Wave Propagation*. 1st ed. London (UK): The Institution of Electrical Engineers, 2000. ISBN: 978-0852967645

[36] RADIOCOMMUNICATION SECTOR OF INTERNATIONAL TELECOMMUNICATION UNION (ITU-R). *Recommendation ITU-R P.452-16: Prediction Procedure for the Evaluation of Interference Between Stations on the Surface of the Earth at Frequencies Above About 0.1 GHz*. [Online] Cited 2025-07-21. Available at: https://www.itu.int/rec/R-REC-P.452-16-201507-S/en

[37] RADIOCOMMUNICATION SECTOR OF INTERNATIONAL TELECOMMUNICATION UNION (ITU-R). *Recommendation ITU-R P.1812-6: A Path-Specific Propagation Prediction Method for Point-to-Area Terrestrial Services in the Frequency Range 30 MHz to 6000 MHz*. [Online] Cited 2025-07-21. Available at: https://www.itu.int/rec/R-REC-P.1812-6-202109-S/en

[38] LS TELCOM AG. *CHIRplus_BC–Broadcast Network Planning Tool*. [Online] Cited 2025-07-22. Available at: https://www.lstelcom.com/en/products/network-planning-tools/broadcast-mobile-tv/

[39] OPENTOPOGRAPHY. *Copernicus GLO-30 Digital Elevation Model*. [Online] Cited 2025-07-22. Available at: https://portal.opentopography.org/raster?opentopoID=OTSDEM.032021.4326.3

[40] THE MATHWORKS, INC. *MATLAB, Version R2023b*. [Online] Cited 2025-07-22. Available at: https://www.mathworks.com/products/matlab.html

[41] INTERNATIONAL TELECOMMUNICATION UNION. *Software, Data and Validation Examples for Ionospheric and Tropospheric Radio Wave Propagation and Radio Noise*. [Online] Cited 2025-07-22. Available at: https://www.itu.int/en/ITU-R/study-groups/rsg3/Pages/iono-tropo-spheric.aspx

[42] OZGUN, O., SAHIN, V., ERGUDEN, M. E., et al. PETOOL v2.0: Parabolic equation toolbox with evaporation duct models and real environment data. *Computer Physics Communications*, 2020, vol. 256, p. 1–9. DOI: 10.1016/j.cpc.2020.107454

[43] CURRY, T., ABBAS, R. 5G coverage, prediction, and trial measurements. *arXiv Preprint*, 2020, p. 1–4. DOI: 10.48550/arXiv.2003.09574

[44] WACKERLY, D., MENDENHALL, W., SCHEAFFER, R. L. *Mathematical Statistics with Applications*. 7th ed. Boston (USA): Cengage Learning, 2014. ISBN: 978-0-495-11081-1

[45] AGUILAR, F. J., AGUILAR, M. A., AGÜERA, F., et al. Effects of terrain morphology, sampling density, and interpolation methods on grid DEM accuracy. *Photogrammetric Engineering & Remote Sensing*, 2005, vol. 71, no. 7, p. 805–816. DOI: 10.14358/PERS.71.7.805

[46] OPPENHEIM, A. V., WILLSKY, A. S., NAWAB, S. H. *Signals and Systems*. 2nd ed. Upper Saddle River (NJ, USA): Prentice Hall, 1997. ISBN: 0-13-8147574

About the Authors . . .

Tamás István UNGER (corresponding author) is a PhD candidate in Informatics at Széchenyi István University and a spectrum management expert at the National Media and Infocommunications Authority (NMHH), Hungary. His research focuses on radiowave propagation models for emerging technologies and frequency bands, including the evaluation and enhancement of empirical and hybrid models through simulation and machine learning. He has expertise in numerical methods, MATLAB-based modeling, and international frequency coordination. He holds degrees in Electrical Engineering (BSc, MSc) and Mathematics (BSc), and speaks English and Slovak.

Miklós KUCZMANN is Full Professor at Széchenyi István University and Head of the Doctoral School of Multidisciplinary Engineering Sciences. His research focuses on numerical electromagnetic field modeling, hysteresis phenomena, and electrical machine simulation. He holds a PhD, habilitation, and the Doctor of Science (DSc) title from the Hungarian Academy of Sciences. He has served as dean, department head, and currently chairs the Scientific Committee on Electrical Engineering of the Hungarian Academy of Sciences. He is a member of the Hungarian Academy of Engineering and teaches across BSc, MSc, and PhD levels.